Substituted 1,5-Diphenyl-3-benzothiazol-2-yl-Δ^2-pyrazolines: Synthesis, X-ray Structure, Photophysics, and Cation Complexation Properties

Knut Rurack,*,†,‡ Julia L. Bricks,§ Burkhard Schulz,‡ Michael Maus,⊥ Günter Reck,‡ and Ute Resch-Genger‡

Institut für Physikalische und Theoretische Chemie, Humboldt Universität zu Berlin, Bunsenstrasse 1, D-10117 Berlin, Germany; Bundesanstalt für Materialforschung und -prüfung (BAM), Richard-Willstätter-Strasse 11, D-12489 Berlin, Germany; Institute of Organic Chemistry, National Academy of Sciences of the Ukraine, Murmanskaya 5, 253660, Kiev-94, Ukraine; and Laboratory for Molecular Dynamics and Spectroscopy (MDS), Department of Chemistry, K. U. Leuven, Celestijnenlaan 200F, B-3001 Heverlee, Belgium

Received: September 23, 1999; In Final Form: April 14, 2000

The spectroscopic properties of 1-phenyl-3-benzothiazol-2-yl-5-(4-R-phenyl)-Δ^2-pyrazolines are strongly dependent on both the electronic nature of the substituent R and solvent polarity. As revealed by spectroscopic studies as a function of solvent polarity as well as temperature, for electron-rich amino donor substituents in polar solvents, deactivation of the strongly emissive charge transfer (CT) state of the basic 1-phenyl-3-benzothiazol-2-yl-Δ^2-pyrazoline chromophore has to compete with a fast intramolecular electron transfer (ET) quenching reaction. In the case of the dimethylamino derivative (R = DMA), the rate constant of ET in acetonitrile was determined to $k_{et} = 3 \times 10^{10}$ s^{-1}. This ET process can be utilized for metal ion sensing by introducing nitrogen containing aza crown ether receptor units to the 4-position of the 5-phenyl group. The spectroscopically determined ET rates of the 5-(*N*-alkyl)anilino substituents, a DMA, a tetrathia- ($AT_4$15C5), and a tetraoxa-monoaza-15-crown-5 (A15C5) group, correlate with electrochemical data and increase in the order $AT_4$15C5 < A15C5 < DMA. The metal ion sensing abilities of the two crowned derivatives are presented, and the different signaling mechanisms include binding to the crown ether in the 4-R-position, chelate formation in the 3-benzothiazol-2-yl-Δ^2-pyrazoline moiety, and electrophotochemical detection. Furthermore, the rigid "pseudo spiro" geometry of the molecules, which holds the three substituents of the central Δ^2-pyrazoline ring in a fixed prearrangement, was confirmed by X-ray structure analysis.

1. Introduction

Fast electron transfer (ET) processes in fluorophore-spacer electron donor (or acceptor) systems harbor an enormous potential in molecular signaling and switching technology.[1] Depending on the redox potential of the molecular subunits and their chemical nature, various photoinduced reactions entail a "switching on" or "off" of fluorescence or can be utilized to construct sophisticated molecular devices with "logic" functions.[2] Moreover, the efficiency of an ET process depends not only on the "ET-active" molecular fragments but also on the chemical nature, the length, rigidity, and local geometry of the spacer group.[3] Whereas, for instance, long and flexible spacers can lead to "self-harpooning" ET interactions,[4] short and rigid spacer units can be used to design electronically decoupled molecular systems in a fixed arrangement.[5,6] In the latter systems, the amount of electronic interaction between nearly perpendicular subunits critically determines the ET quenching rate.[7]

Utilization of such ET processes in cation complexing fluorescent probes can yield highly efficient fluorescent sensor molecules[8,9] which allow the determination of nonfluorescent metal ions with increased sensitivity compared with probes utilizing only intramolecular charge transfer (ICT)-based absorbance/fluorescence changes.[10,11] Binding of a cation to the receptor of such an ET probe is accompanied by a large change in fluorescence intensity due to complexation-induced inhibition or acceleration of a nonradiative process, respectively ("off/on" or "on/off" sensing), rather than by cation-induced spectral shifts.[8,9] On the other hand, for ICT probes, despite pronounced spectral shifts in both absorption and emission, only small changes in fluorescence intensity and lifetime are observed.[10,11]

Up to now, mainly fluorescent ET probes for alkali and alkaline-earth metal ions[8,9,12−14] have been described. However, fluorescent probes for the detection of heavy and transition metal ions require a more refined design, since selective complexation of these chemically often closely related ions is more difficult and interfering effects (heavy atom effect, paramagnetism)[15,16] induced by ion complexation have to be avoided. The carefully directed receptor design[17] for selective complexation of such metal ions as Ag^I, Hg^{II}, or Cu^{II} can be achieved by employing, e.g., monoaza macrocycles with "soft" sulfur instead of "hard" oxygen donor atoms[17−19] (in terms of Pearson's concept of "hard and soft acids and bases" (HSAB)[20]). On the other hand, heavy atom effects can be minimized and the fluorescence enhancement factor (FEF) can well be optimized if an intramolecular electron transfer (ET) between two electronically decoupled electron donor and acceptor units, one of which consists of the receptor group, is utilized to build modular fluorescent probes for heavy and transition metal ions.[2d,21−29]

† Humboldt Universität zu Berlin.
‡ Bundesanstalt für Materialforschung und -prüfung.
§ National Academy of Sciences of the Ukraine.
⊥ K. U. Leuven.

10.1021/jp993404q CCC: $19.00
Published on Web 06/10/2000

SCHEME 1: Chemical Structures and Labeling of the 1,3,5-Triaryl-Δ^2-pyrazolines Investigated

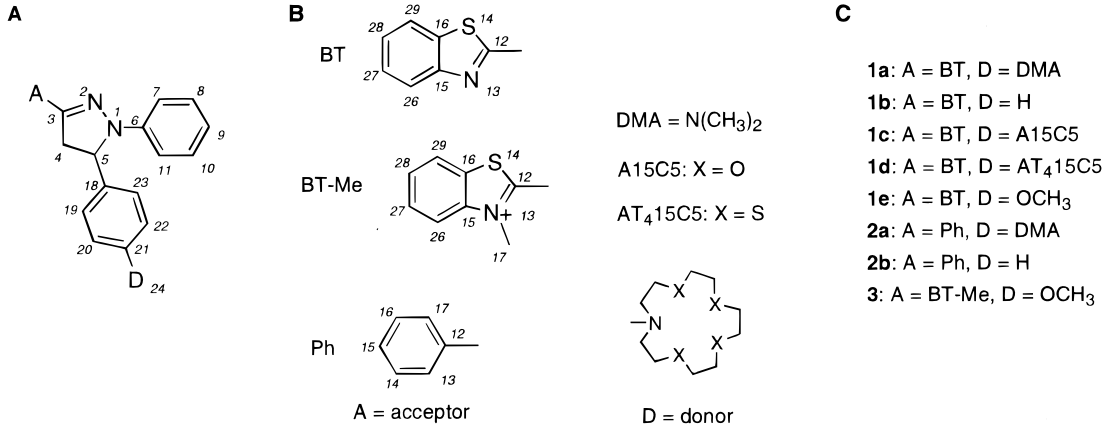

1,3,5-Triaryl-Δ^2-pyrazolines, with their rigid but only partly unsaturated central Δ^2-pyrazoline ring, are known for their bright fluorescence.[30] The ICT chromophore itself involves only three atoms of the pyrazoline five-membered ring and two aryl (Ar) moieties in 1- and 3-position, i.e., the $\pi p \pi$ conjugated Ar—C(3)R═N(2)—N(1)R—Ar fragment (Scheme 1A).[31−34] The 5-substituent is separated by a "bridged ethylene group", i.e., the CH_2—CHR group of the pyrazoline ring, the reduced flexibility of this arrangement preventing pronounced electronic interaction in the ground state but enabling interaction via long-range processes in the excited state, i.e., electron transfer. The fluorescence quantum yields of such molecules depend on both the 1,3-(ICT) fragment and the isolated 5-substituent.[35a] Without a strong donor at the 5-position, rather intense fluorescence bands ($\phi_f \sim 0.8$) are found, but introduction of a strong donor (e.g., amino; or a strong acceptor, e.g., nitro or carboxyl) group at this position causes considerable fluorescence quenching in polar solvents with the ICT characteristics, i.e., absorption and emission bands, remaining unchanged.[35a] Accordingly, applications of 1,3,5-triphenyl-Δ^2-pyrazoline derivatives as fluorescent probes have been described,[33,36,37] such probes showing complexation-induced fluorescence enhancement factors (FEFs) of 10−70.[2a,8,33,37]

Here, we present a new series of 1,3,5-triaryl-Δ^2-pyrazolines with the benzothiazole moiety at the 3-position (Scheme 1), this substitution promising to shift the absorption and emission spectra into the visible (vis) region of the spectrum. Furthermore, the 5-phenyl substituent was equipped with an oxidizable receptor group, a tetrathia- or a tetraoxa-monoaza crown ether, in order to enable a cation-sensitive intramolecular excited state ET process.

In the field of rational molecular design, the mechanistical characterization as well as the correlation of spectroscopic, electrochemical, quantum chemical, and structural data is very helpful. In the case of these 1,3,5-triaryl-Δ^2-pyrazolines, the photoinduced intramolecular processes are studied as a function of solvent polarity as well as temperature and are analyzed by quantum chemical calculations to get insight into the ET process predicted for that family of compounds with electron donor−acceptor interactions. Furthermore, the crystal structures and electrochemical properties (of some) of the dyes are described. The resulting implications for an analytical application of the ET probes **1c** and **1d** are discussed and their complexation behavior toward the alkali and alkaline-earth metal ions Li^I, Na^I, K^I, Mg^{II}, Ca^{II}, Sr^{II}, and Ba^{II} as well as the heavy and transition metal ions Ag^I, Cu^I, Cu^{II}, Ni^{II}, Co^{II}, Zn^{II}, Cd^{II}, Hg^{II}, and Pb^{II} in acetonitrile at 298 K is presented. For a better understanding of the complexation experiments, model compound **3** is also included in some of the studies.

2. Experimental Section

2.1. Materials. Metal perchlorates purchased from Merck, Acros, and Aldrich were of highest purity available and dried in a vacuum oven before use[38] (see also Supporting Information, section S1). All the solvents employed were of UV spectroscopic grade. For the determination of the complex stability constants, acetonitrile was distilled from CaH_2 prior to use. The following abbreviations for the solvents are used throughout the text: methanol, MeOH; ethanol, EtOH; acetonitrile, MeCN; tetrahydrofuran, THF; diethyl ether, Et_2O; cyclohexane, CH.

2.2. Synthesis. General Methods. The chemical structures of the synthesized compounds were confirmed by elemental analysis, ^{1}H NMR, ^{13}C NMR, and MS and their purity was checked by reversed phase HPLC (HPLC set up from Merck-Hitachi; RP18 column; acetonitrile/water = 75/25 as eluent) employing UV detection (UV detector from Knaur; fixed wavelength at 310 nm). NMR spectra were obtained with a 500 MHz NMR spectrometer Varian $Unity_{plus}$ 500. The mass spectra were recorded on a Finnigan MAT 95 spectrometer with an ESI−II/APCI-Source for electrospray ionization and the base peaks $[M + Na]^+$ were determined. Descriptions of the syntheses and analytical data are provided in Supporting Information, section S2.

2.3. Steady-State Absorption and Fluorescence Spectroscopy. UV/vis spectra were recorded on a Carl Zeiss Specord M400/M500 absorption spectrometer. For the temperature-dependent absorption experiments, a Bruins Instruments Omega 10 spectrophotometer was employed. Steady-state emission spectra were recorded on a Perkin-Elmer LS50B and a Spectronics Instruments 8100 spectrofluorometer. For the fluorescence experiments, only dilute solutions with an optical density (OD) below 0.01 at the excitation wavelength (OD < 0.04 at the absorption maximum) were used. The relative fluorescence quantum yields (ϕ_f) were determined by adjusting the optical densities of the solutions at the excitation wavelengths to 0.1 ± 0.001 in a 100 mm absorption cell. These solutions were then transferred to a 10 mm quartz cell and the fluorescence measurements were performed with a 90° standard geometry and polarizers set at 54.7° (emission) and 0° (excitation). Fluorescein 27 in 0.1 N NaOH ($\phi_f = 0.90 \pm 0.03$),[39a] coumarin 1 in ethanol ($\phi_f = 0.5$),[39b] and coumarin 153 in ethanol ($\phi_f = 0.4$)[39b] were used as fluorescence standards. All the fluorescence spectra presented here are corrected for the spectral response of the detection system (calibrated quartz halogen lamp placed

inside an integrating sphere; Gigahertz-Optik) and for the spectral irradiance of the excitation channel (calibrated silicon diode mounted at a sphere port; Gigahertz-Optik). The fluorescence quantum yields were calculated from six independent measurements and the uncertainties of the measurement were determined to ±5% (for $\phi_f > 0.2$), ±10% (for $0.2 > \phi_f > 0.02$), ±20% (for $0.02 > \phi_f > 5 \times 10^{-3}$), and ±30% (for $5 \times 10^{-3} > \phi_f$), respectively.

2.4. Time-Resolved Fluorescence Spectroscopy. Fluorescence lifetimes (τ_f) were measured employing a unique laser impulse fluorometer with picosecond time resolution described elsewhere.[40] The sample was excited with the second harmonic output (LBO crystal) of a regenerative mode locked argon ion laser pumped Ti:sapphire laser at a repetition rate of either 82 or 4 MHz (reduction by synchronized pulse selection). The fluorescence was collected at right angles (polarizer set at 54.7°; monochromator with spectral bandwidths of 4, 8, and 16 nm), and the fluorescence decays were recorded with a time-correlated single photon counting setup and a time division of 5.2 ps channel^{-1} (82/4 MHz version) or 52.6 ps channel^{-1} (4 MHz version). The corresponding experimental accuracies were ±3 ps and ±0.04 ns, respectively. The laser beam was attenuated using a double prism attenuator from LTB, and typical excitation energies were in the nanowatt to microwatt range (average laser power). The excitation energies were checked and adjusted with a calibrated Si diode (model 221 with 100:1 attenuator 2550, Graseby) and an optometer (model S370, Graseby). In a typical experiment, the pulse peak power was 3×10^{-3} W (5×10^{-2} W) in the 82 MHz (4 MHz) mode. For example, concerning a typical measurement at 400 nm the sample was excited with ca. 10^5 photons per pulse. The instrumental response function of the system was typically 30 ps (full width at half-maximum). Temporal calibration of the experimental setup was checked with pinacyanol in ethanol ($\tau_f = 13 \pm 1$ ps),[41a] rose bengal in methanol ($\tau_f = 0.50$ ns ± 0.02 ns),[41b] and fluorescein 27 in 0.1 *N* NaOH ($\tau_f = 4.50$ ns ± 0.03 ns).[41c] For the estimation of the color shift (wavelength-dependent temporal response of the detection system) between the instrumental response function and the actual fluorescence decay, the fluorescence of coumarin 1 (in ethanol), coumarin 153 (in ethanol), and fluorescein 27 (in 0.1 N NaOH) were quenched by saturation with potassium iodide and their decay profiles were recorded at the corresponding emission wavelengths.

The fluorescence lifetime profiles were analyzed with a PC using the software packages IBH Decay Analysis Software V4.2 (IBH Consultants Ltd.) and Global Unlimited V2.2 (Laboratory for Fluorescence Dynamics, University of Illinois). The goodness of the fit of the single decays, judged by reduced chi-squared (χ_R^2), the autocorrelation function *C(j)* of the residuals, and the Durbin−Watson parameter (DW), was always in the range of $\chi_R^2 < 1.2$ and DW > 1.8. Within the global analysis of the decays recorded at different emission wavelengths, the decay times of the species are linked while the program varies the preexponential factors and lifetimes until the changes in the error surface (χ^2 surface) are minimal; i.e., convergence is reached. The fitting results are judged for every single decay (local χ_R^2) and for all the decays (global χ_R^2). Except as otherwise indicated, the errors for all the measurements presented here were below global $\chi_R^2 = 1.2$.

When biexponential decay kinetics are found and an excited state reaction can be excluded, i.e., in the case of ground state heterogeneity, wavelength-resolved fluorescence decay profiles can be analyzed globally according to eq 1 ($I_{tot}(\lambda,t) = \sum_i a_i(\lambda) e^{-t(\tau_i)^{-1}}$: total fluorescence intensity, $a_{rel}{}^i = a_i/\sum_i a_i$: relative amplitude, $\Phi_{rel}{}^i = a_i\tau_i/\sum_i a_i\tau_i$: fractional intensity, $DAS_i(\lambda)$: decay-associated spectrum, $F_{SS}{}^{tot}$: steady-state fluorescence intensity).[42]

$$DAS_i(\lambda) = \frac{a_i(\lambda) F_{SS}{}^{tot}(\lambda)}{\sum_i a_i(\lambda)\tau_i} \quad (1)$$

2.5. Temperature-Dependent Measurements. The temperature-dependent measurements were performed with a continuous flow He cryostat CF 1204 from Oxford Instruments. Liquid helium was pumped from a storage container via a transfer tube (GFS 300, Oxford Instruments) and flow control (VC 30, Oxford Instruments) by a gas flow pump (GF 2, Oxford Instruments) through the cryostat. The temperature was externally controlled by heating and flow adjustment with the temperature controller ITC 4 from Oxford Instruments. The temperature in the sample rod was monitored via the temperature-dependent resistance of a sensor which was calibrated with a Peltier element. When cooling, the temperature was gradually decreased in steps of 15 or 20 K (at $T > 170$ K) with equilibration times of 20 min at every point of measurement. Then the sample was immediately chilled (with liquid He to $T = 10$ or 30 K), equilibrated for 40 min, and heated in steps of 20 K (equilibration time of 20 min) to 170 K.

2.6. Complex Stability Constants. The complex stability constants reported here were determined from both absorption (in 50 or 100 mm absorption cells) and fluorescence measurements. The complex stability constants *K* were measured by titrating a dilute solution (typically 10^{-6} M) of ligand by adding aliquots of metal ion solution (c_{M0} titration). For the fit of the complexometric titration data (employing Origin V5.0, Microcal Software, Inc.), the following equations apply (*X*, absorption or fluorescence intensity; *a*, *b*, constants; c_M, c_L, free metal, free ligand, and complex concentrations; $c_{Y0,}$ total concentrations) and the theoretical background is discussed in more detail in ref 43.

When X_{lim} is not known, eq 2 allows for the graphical determination of *K* and for efficient complexation, when $c_M \sim c_{M0}$ is not valid anymore, eq 3 can be used.[43]

$$\frac{X_0}{X - X_0} = \frac{a}{b - a}\frac{1}{K c_M} + 1 \quad (2)$$

$$X = X_0 + \frac{X_{lim} - X_0}{2c_{L0}}\left\{c_{L0} + c_{M0} + \frac{1}{K} - \left[\left(c_{L0} + c_{M0} + \frac{1}{K}\right)^2 - 4c_{L0}c_{M0}\right]^{1/2}\right\} \quad (3)$$

The reported values are mean values of at least two measurements with correlation coefficients >0.99.

2.7. Quantum Chemical Calculations. Geometry optimizations were performed employing the semiempirical AM1 method (gradient < 0.01; HyperChem V4.0 and 4.5, Hypercube, Inc.).[44] Rotational energy barriers were calculated by iterative twisting of the bond(s) of interest. The energies of the corresponding perpendicular structures were found by optimizing the geometry with the exception of a single fixed dihedral angle of 90°. Transition energies were calculated on the basis of the corresponding ground-state geometries and 1SCF calculations with a CI of 8 by the methods AM1 (Ampac V5.0 and V6.55, Semichem, Inc.) and ZINDO/S.[45]

2.8. X-ray Structure Analysis. The X-ray data of **1b**, **2a**, and **3** were collected on a Siemens SMART diffractometer at 293 K using Mo Kα radiation ($\lambda = 0.710\ 73$ Å) monochromatized by a graphite crystal. The structures were solved by direct methods and refined by full-matrix least-squares calculations (SHELXTL). The hydrogen atoms of all the structures were introduced in their calculated positions and refined using Riding models.[46]

2.9. Cyclic Voltammetry. The cyclic voltammograms were obtained in acetonitrile/0.1 M Bu_4NPF_6 solution with an Amel 553/Amel 568 system in a standard single compartment three electrode design (Pt working electrode and counter electrode, Ag/AgCl quasireference electrode). Ferrocene was used as an internal standard, and measurements were performed under inert gas with a scan rate of either 1000 or 250 mV s^{-1} (for **1b**). All the potentials given in the text are in mV vs Fc/Fc^+.

3. Results and Discussion

3.1. Structural and Photophysical Studies. 3.1.1. X-ray Crystallography. The total X-ray structures of the (*R*) stereoisomers of the three molecules are collected in Figure 1 and the relevant geometrical parameters are combined in Table 1. All the three molecules crystallize as a racemate. The 1,3-diaryl-Δ^2-pyrazoline chromophore is nearly planar in the Ar—C(3)R═N(2)—N(1) fragment of **1b**, **2a**, and **3** (see dihedral angles of the molecular planes in Table 1) and a partly tetrahedral conformation at N(1) only occurs for **2a**, manifested by a sum of the bond angles at N(1) of 351.9° (Table 1). In this case, the lone electron pair of N(1) and the hydrogen atom at C(5) point into opposite directions. Whereas **2a** shows a pronounced bond length alternation in the C(6)—N(1)—N(2)—C(3)—C(12) fragment, the stronger conjugation of the Δ^2-pyrazoline chromophore in **1b** and especially **3** follows from the double bond character of the bonds C(3)—C(12) (1.450 and 1.432 Å) and N(1)—N(2) (1.365 and 1.361 Å). Furthermore, the bond N(1)—C(6) (ca. 1.40 Å) displays similar features.[47] For **3**, where the Ar—C(3)R═N(2)—N(1)—Ph unit is most planar ($\theta_{1-2} = 2.2°$ and $\theta_{1-3} = 6.5°$, Table 1), the bond length alternation is further reduced, indicating the strongest delocalization for this compound. Concerning **1b** and **3**, alkylation of N(13) does not only increase the conjugation in the chromophore but leads to a change in conformation as well, i.e., the BT moiety and the Δ^2-pyrazoline ring are in N(2)—N(13) anti conformation for **1b** but the syn conformer is favored for **3**. The results obtained for the basic chromophore of **2a** are generally in good agreement with the structural data of 1,3-diphenyl-Δ^2-pyrazoline reported by Duffin[48] despite the distortions imposed by the 5-substituent (Table 1).

Compared to the three aryl substituents, the central Δ^2-pyrazoline ring shows a reduced planarity for all the three compounds (cf. description of molecular planes in Table 1). The dihedral angle between the planes of the 5-substituent and the Δ^2-pyrazoline ring amounts to ca. 78° (Table 1), resulting in a tilted, "pseudo spiro" arrangement of both molecular fragments. Regarding the degree of pyramidalization at the dimethylamino (DMA) (or aza crown) nitrogen atom, the sum of the bond angles at N(24) equals 358.4° for **2a**, very similar to the values found by us for *N*-phenyltetraoxamonoaza-15-crown-5 (*N*-phenyl-A15C5) and *N*-phenyltetrathiamonoaza-15-crown-5 (*N*-phenyl-$AT_4$15C5).[49] Accordingly, the bond C(21)—N(24) shows a certain double bond character (1.390 Å).

3.1.2. Absorption and Emission at 298 K. The photophysical data of the compounds investigated are collected in Table 2. The first prominent features which render the benzothiazol-2-yl (BT)-substituted dyes analytically more valuable than most of their triphenyl derivatives are their red-shifted absorption and emission bands accompanied by high fluorescence quantum yields (for compounds without a 5-*p*-anilino donor). For example, in acetonitrile, the absorption band is centered at ca. 25 000 cm^{-1} and emission occurs at ca. 19 500 cm^{-1}, while for **2a**, the corresponding transitions are found at 27 700 cm^{-1} and 21 300 cm^{-1}, respectively. As derived from the quantum chemical calculations below (section 3.1.4), the nature of the electronic transition ($\pi\pi^*$ nature) involves an intramolecular charge transfer from the 1-Ph—N(1) donor to the Ar—C(3)═N(2) acceptor. Along with the CT, increased charge densities are found for the pyrazoline ring atoms N(2) and C(3) in the

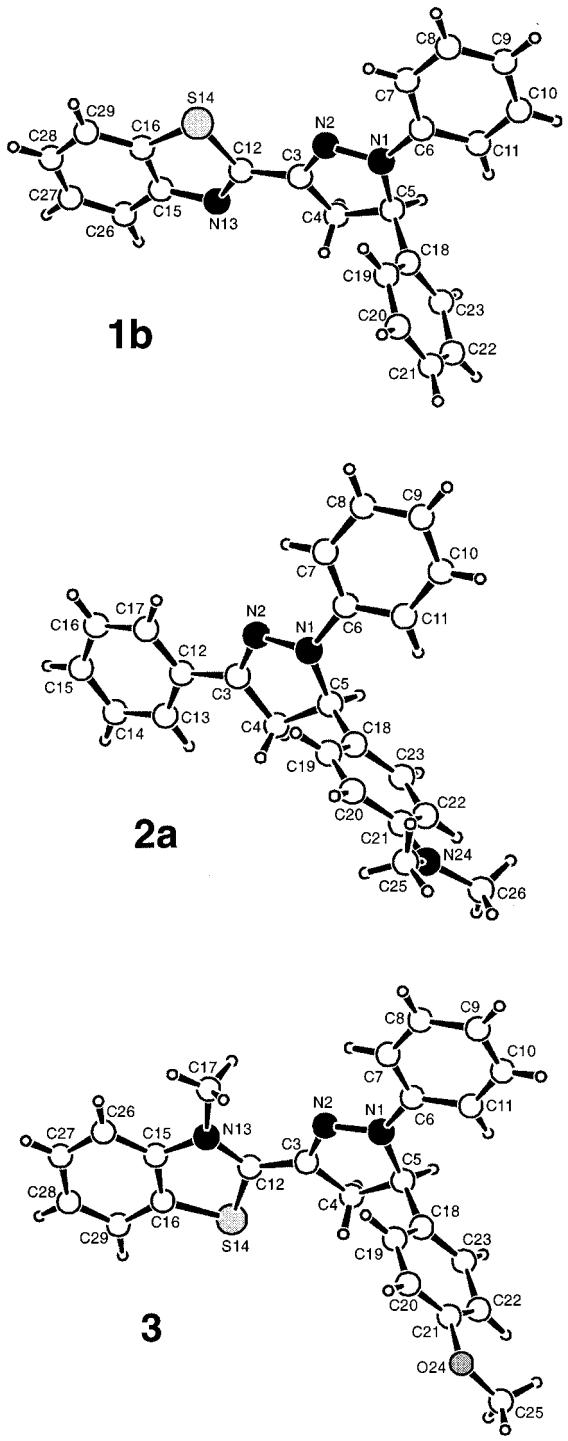

Figure 1. X-ray structures of the (*R*) stereoisomers of **1b**, **2a**, and **3**.

TABLE 1: Selected Bond Lengths (Å), Angles (deg), and Dihedral Angles of the Molecular Planes (deg) of the X-ray Structures of 1b, 2a, and 3

	1b	2a	3
N(1)−N(2)	1.365	1.394	1.361
N(2)−C(3)	1.291	1.292	1.327
C(3)−C(12)	1.450	1.478	1.432
N(1)−C(6)	1.394	1.424	1.407
N(1)−C(5)	1.477	1.477	1.497
C(5)−C(18)	1.512	1.497	1.516
C(3)−C(4)	1.487	1.490	1.505
C(4)−C(5)	1.540	1.550	1.552
N(2)−N(1)−C(5)	113.4	113.3	113.2
C(5)−N(1)−C(6)	125.6	122.5	126.0
N(2)−N(1)−C(6)	120.6	116.1	120.5
Σ	359.6	351.9	359.7
θ_{1-2}[a]	12.9[b]	20.9[b]	2.2[b]
θ_{1-3}[a]	3.2[b]	5.2[b]	6.5[b]
θ_{1-4}[a]	81.0[b]	76.5[b]	81.1[b]

[a] Plane 1 = atoms N(1) to C(5); plane 2 = C(6) to C(11); plane 3 = C(12) to C(16) and C(26) to C(29); plane 4 = C(18) to C(23). [b] Atomic deviations from the planes given in ref 110.

TABLE 2: Spectroscopic Data of the Substituted 1,3,5-Triaryl-Δ^2-pyrazolines at 298 K

	solvent	$\tilde{\nu}$(abs) (10^3 cm^{-1})	$\epsilon[\tilde{\nu}(\text{abs})]$ (10^3 M^{-1} cm^{-1})	$\tilde{\nu}$(em) (10^3 cm^{-1})	$\Delta\tilde{\nu}$(abs−em) (cm^{-1})	ϕ_f	τ_f (ns)
1a	MeOH	24.51	27.7	19.36	5150	0.003	0.03
	MeCN	24.94	29.0	19.34	5600	0.006	0.03
	acetone	24.81	28.4	19.60	5210	0.08	0.20
	THF	24.75	28.5	19.80	4950	0.55	3.00
	Et_2O	25.00	27.9	20.30	4700	0.86	4.02
	toluene	24.57	29.8	20.12	4450	0.84	3.39
	hexane	25.13	25.8	21.03	4100	0.78	3.31
1b	MeOH	24.81	28.8	19.17	5640	0.38	2.54
	MeCN	25.13	29.4	19.61	5520	0.72	4.02
	acetone	25.06	29.3	19.73	5330	0.75	3.91
	THF	24.88	29.4	19.90	4980	0.71	3.88
	Et_2O	25.19	25.7	20.46	4730	0.87	4.17
	toluene	24.81	28.2	20.33	4480	0.84	3.45
	hexane	25.32	24.9	21.19	4130	0.73	3.32
1c	MeOH	24.51	26.3	19.42	5090	0.006	0.05[a]
	MeCN	25.00	28.2	19.52	5480	0.016	0.11[a]
	toluene	24.57	27.3	20.00	4570	0.85	3.34
	hexane	25.06	25.1	21.05	4010	0.75	3.27
1d	MeCN	24.94	29.7	19.47	5470	0.10	1.07[a]
	toluene	24.63	27.8	20.26	4370	0.87	3.46
1e	MeOH	24.75	26.1	19.17	5580	0.36	2.42
	MeCN	25.00	27.5	19.57	5430	0.77	4.05
	hexane	25.25	25.2	21.16	4090	0.85	3.32
2a	MeOH	27.93	17.7	20.54	7390	0.19	1.56
	MeCN	27.70	19.0	21.34	6360	0.69	4.19
	hexane	27.70	18.8	23.01	4690	0.52	2.90
2b	MeOH	28.09	18.9	20.81	7280	0.38	n.d.[b]
	MeCN	28.09	19.1	21.50	6590	0.62	4.33[c]
	CH[d]	28.1	n.r.[b]	23.4	4730	0.82	n.r.[b]

[a] $\langle\tau_f\rangle$ calculated according to ref 111; for explanation see text. [b] n.d. = not determined, n.r. = not reported. [c] Reference 55. [d] Reference 35a.

first excited singlet state. As can be derived from the data in Table 2 and Figures 2 and 3, the position of the bands is thus significantly influenced by the 1-*p*- and 3-*p*-substituents of the pyrazoline ring whereas the fluorescence quantum yield depends on the para-substituent at all three positions.[33b,35a,50] For all the solvents employed, the absorption and fluorescence excitation spectra of the dyes investigated match.

Steady-State Spectra. A comparison of the absorption spectra of **1b** with those of the anilino-substituted derivatives (e.g., **1a**) in Figure 2 reveals that for the 5-*p*-amino-substituted derivatives, the high-energy band of the Δ^2-pyrazoline chromophore and

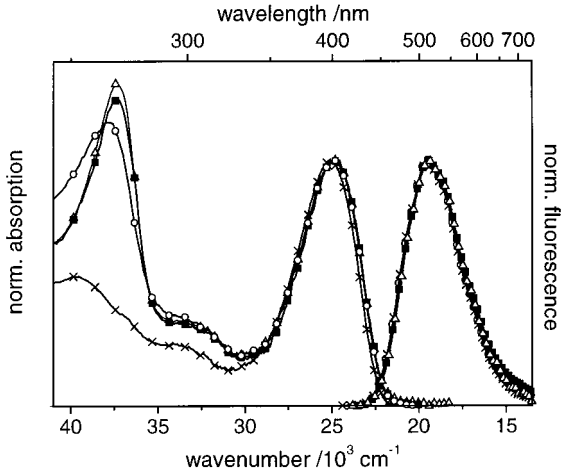

Figure 2. Normalized steady-state absorption and emission spectra of **1a** (○), **1b** (×), **1c** (■), and **1d** (△) in acetonitrile at 298 K.

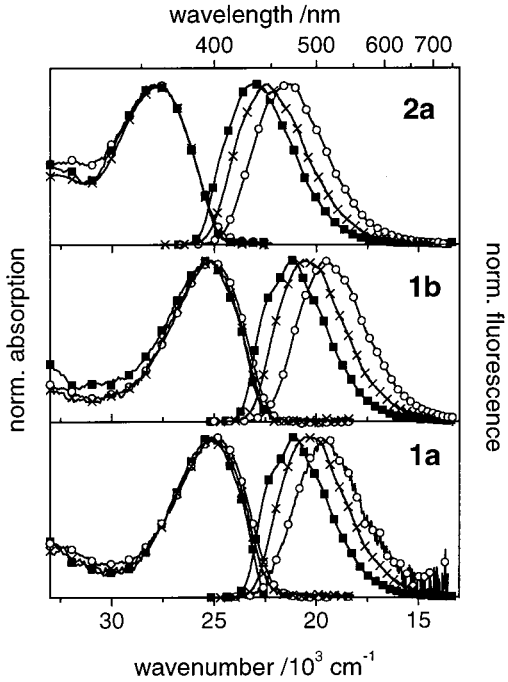

Figure 3. Normalized steady-state absorption and emission spectra of **1a**, **1b**, and **2a** in *n*-hexane (■), diethyl ether (×), and acetonitrile (○) at 298 K.

the most intense transition in the alkylated anilino chromophore (at ca. 37 700 cm^{-1}) are superimposed. In all the solvents studied here, both the absorption and emission spectrum show no vibrational structure and even in *n*-hexane a slightly structured band is only seen in the emission spectrum. The Stokes shift increases with solvent polarity indicating a higher dipole moment in the excited state than in S_0 (Figure 3) and in aprotic solvents, all the dyes have high fluorescence quantum yields. Thus, in all the solvents, emission is due to an allowed charge-transfer transition $S_1(CT) \rightarrow S_0$. These observations are in agreement with those reported by other research groups for 1,3-di- and 1,3,5-triaryl-Δ^2-pyrazolines.[32,33,36,50−55] The negligible spectroscopic effect of various 5-*p* donor substituents is even observed for the bulky crown ether groups and gives further evidence for the rigidity of the "Δ^2-pyrazoline bridge" and the prearrangement of 1-, 3-, and 5-substituents in a conformation preventing sizable orbital overlap.

Transition Dipole Moments and Geometry of the States. A possible change of the nature from the absorbing to the emitting

TABLE 3: Photophysical Parameters of the Substituted 1,3,5-Triaryl-Δ²-pyrazolines at 298 K

	solvent	k_f^{obs} (10^8 s^{-1})	k_{nr}^{obs} (10^8 s^{-1})	k_f^{calc} (10^8 s^{-1})	k_f^{obs}/k_f^{calc}
1a	MeOH	1.4	450	1.7	0.78
	MeCN	1.8	300	1.9	0.94
	Et_2O	2.1	0.4	2.0	1.06
	hexane	2.4	0.7	2.0	1.18
1b	MeOH	1.5	2.4	1.7	0.87
	MeCN	1.8	0.7	1.9	0.93
	Et_2O	2.1	0.3	1.9	1.09
	hexane	2.3	0.8	1.9	1.21
1c	hexane	2.3	0.8	2.1	1.08
1d	toluene	2.5	0.4	2.3	1.09
1e	MeOH	1.5	2.6	1.7	0.89
	MeCN	1.9	0.6	1.9	0.98
	hexane	2.4	0.6	2.2	1.12
2a	MeOH	1.2	5.2	1.3	0.94
	MeCN	1.6	0.7	1.6	1.00
	hexane	1.8	1.7	1.8	1.01

state, as might be induced by excited-state relaxations of the average twist angle around bonds N(1)−C(6) and C(3)−C(12), can be derived from a comparison of the radiative rate constant observed k_f^{obs} (eq 4a) and k_f^{calc} (eq 5a), the corresponding rate constant calculated from the absorption spectra (Table 3).

$$k_f^{obs} = \frac{64\pi^4}{3h} n^3 \tilde{\nu}_{em}^{\ 3} |M_{em}|^2 \quad \text{with} \quad |M_{em}|^2 = \frac{3h}{64\pi^4 n^3} \frac{\phi_f}{\tau_f \tilde{\nu}_{em}^{\ 3}} \tag{4a,b}$$

$$k_f^{calc} = \frac{64\pi^4}{3h} n^3 \tilde{\nu}_{em}^{\ 3} |M_{abs}|^2 \quad \text{with}$$

$$|M_{abs}|^2 = \frac{3hc_0 \ln 10}{8\pi^3 N_A n} \int_{band} \frac{\epsilon(\tilde{\nu}_{abs})\, d\tilde{\nu}_{abs}}{\tilde{\nu}_{abs}} \tag{5a,b}$$

Here, M_{abs} and M_{em} are the transition dipole moments obtained by analyzing steady-state and dynamic photophysical data according to eqs 4b and 5b,[56,57] n is the refractive index of the solvent, and the other constants include speed of light in a vacuum (c_0), Planck constant (h), and Avogadro constant (N_A). The ratios k_f^{obs}/k_f^{calc} of 1.1−1.2 (for the 3-benzothiazol-2-yl-substituted derivatives) in *n*-hexane as compared to ratios of 0.93−0.98 in acetonitrile most probably suggest the involvement of both electronic solute−solvent interactions and/or a relaxation of the initially excited Franck−Condon state to a slightly more planar conformation of the emitting CT state (Table 3).[58] However, the differences in conformation seem to be rather small. In contrast, the influence of protic solvents is well reflected by a more distinct decrease in k_f^{obs}/k_f^{calc} for **1a**, **1b**, **1e**, and **2a** upon going from acetonitrile to methanol (Table 3). Here, the ratio of 0.78 for **1a** suggests different intramolecular rearrangements most probably involving hydrogen bond formation.

A similar trend is revealed by the rate constants of radiative and nonradiative deactivation (Table 3), i.e., a slight decrease in k_f ($=\phi_f/\tau_f$) with increasing solvent polarity (and proticity) but a much more pronounced increase in k_{nr} ($=(1-\phi_f)/\tau_f$).

Excited-State Solvatochromism and Dipole Moments. In order to estimate the extent of the CT process and to compare **1a** and **1b** more closely, the spectroscopic data obtained in different solvents were analyzed as a function of solvent polarity employing the Lippert−Mataga formalism (eqs 6 and 7).[59] A plot of the Stokes shift vs the solvent polarity functions

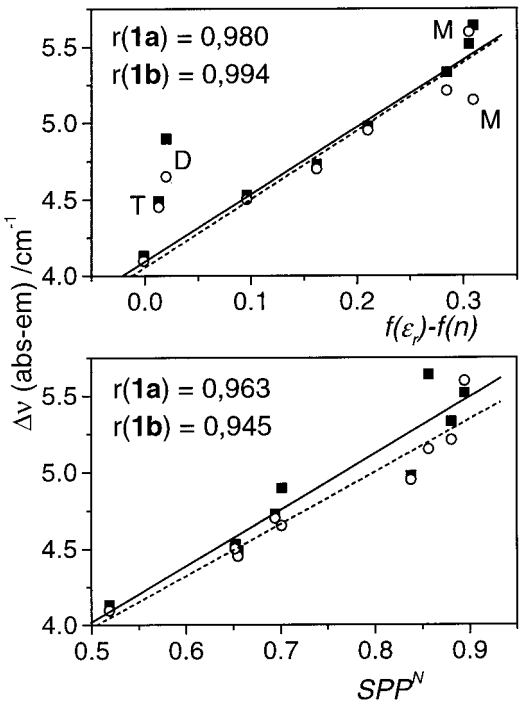

Figure 4. Solvatochromic plots (and fits) according to eq 6 (top) and plots of Stokes shift vs empirical solvent polarity parameter SPP^N (bottom) for **1a** (○, ---) and **1b** (■, —) in the solvents listed in Table 2, di-*n*-butyl ether and 1,4-dioxane. For the fit of the solvatochromic plot the values for toluene (T), 1,4-dioxane (D), and methanol (M) were excluded.

TABLE 4: Dipole Moments Obtained from the Slope of Solvatochromic Plots According to Eqs 6 and 15[a]

	eq	μ_g[b]/D	μ_e/D	$(\mu_e - \mu_g)$/D
1a	6	1.7	14.3	12.6
	15[c]	1.7	10.2	8.5
1b	6	0.8	12.5	11.7
	15[c]	0.8	9.2	8.4

[a] The Onsager cavity radius a_O was taken to 7.1 Å (**1a**) and 6.8 Å (**1b**) on the basis of the AM1 optimized geometry and the method proposed by Edward for spherical molecules.[106] [b] For ground-state geometry optimized by AM1. [c] See ref 62.

$f(\epsilon_r) - f(n)$ (cf. eq 6) is shown in Figure 4 and the dipole moments obtained are included in Table 4.

$$\Delta\tilde{\nu}(abs-em) = \Delta\tilde{\nu}^{vac}(abs-em) + \frac{2(\mu_e-\mu_g)^2}{hc_0 a_O^{\ 3}}(f(\epsilon_r) - f(n)) \tag{6}$$

$$f(\epsilon_r) = \frac{\epsilon_r - 1}{2\epsilon_r + 1} \quad \text{and} \quad f(n) = \frac{n^2 - 1}{2n^2 + 1} \tag{7a,b}$$

Here, $\Delta\tilde{\nu}^{vac}$(abs−em) is the extrapolated Stokes shift in a vacuum, μ_g and μ_e are the ground- and excited-state dipole moments, a_O is the Onsager cavity radius, ϵ_r is the relative permittivity of the respective solvent, and the other constants are given above. Graphical analysis of a plot of the Stokes shift vs the solvent polarity function (last term in eq 6) allows for the determination of $(\mu_e - \mu_g)$ and μ_e (if μ_g is known).[60,61]

The good agreement between the dipole moments obtained for **1a** and **1b** reveals that a 5-*p* donor has a negligible influence on the $S_0 \rightarrow$ CT transition in the 1,3-chromophore. This is also found when taking into account the polarizability of the solute (cf. ref 62) or by applying the empirical SPP^N solvent polarity

scale[63] (Figure 4). Similar magnitudes for Δ^2-pyrazolines are found in the literature, where Güsten et al. reported a value of $(\mu_e - \mu_g) = 11.5$ D for 1-*p*-chlorophenyl-3-*p*-cyanophenyl-Δ^2-pyrazoline (analysis via Bakhshiev's formalism)[32c,64] and Yan et al. found $(\mu_e - \mu_g) = 8.9$ D for 3-*p*-nitro-triphenyl-Δ^2-pyrazoline (analysis via the Bilot−Kawski formalism)[36b,65]. Such a change in dipole moment of ca. 13 D (Table 4) corresponds to a charge separation distance of ca. 3.0 Å equaling a (theoretical) distance from N(1) to the C(3)−C(12) bond reflecting the charge shift within the 1,3-chromophore; in crystalline **1b**, the distances N(1)−C(3) and N(1)−C(12) are 2.148 and 3.543 Å, respectively.

Fluorescence Quantum Yields. Table 2 shows that in contrast to spectral similarity with the reference compound **1b**, the fluorescence quantum yield (ϕ_f) is drastically quenched for the molecules with a strong 5-*p* donor (aniline) in solvents of high polarity (i.e., acetonitrile) and ϕ_f decreases on the order of **1d** ($AT_4$15C5) ≫ **1c** (A15C5) > **1a** (DMA; note that no quenching is observed for the 5-*p*-methoxy derivative **1e**). Furthermore, the efficiency of this (long range) intramolecular quenching process is also very sensitive to the type of the 3-substituent as follows from the data in Table 2. Hence, for a 3-phenyl group (**2a**) quenching is not observed. Since the efficiency of this quenching correlates with the electron donor and acceptor strengths of the 5- and 3-substituents, respectively, we assign this process to an electron transfer (ET) from the D to the A moiety (vide infra, see section 3.1.5).

In protic solvents such as methanol, ϕ_f is even more reduced than in the equipolar but aprotic acetonitrile. This effect occurs regardless of the 3- or 5-substituent and points to an additional quenching of the CT fluorescence. Such phenomena are often encountered for fluorescent CT states[66,67] and have also been observed for other Δ^2-pyrazolines before.[33,35a] Upon excitation, the CT process leads to an increased electron density at N(2) inducing a higher availability of the lone electron pair for hydrogen bonding. Since all the triaryl-Δ^2-pyrazolines display enhanced radiationless deactivation of the excited state in protic solvents, such H-bond formation should occur at N(2). Sterical hindrances seem to play no role here, since a less planar arrangement of the 1-aryl and the Δ^2-pyrazoline moiety (as, e.g., in 1-(2-methylphenyl)[54] or 1-(2,6-dimethylphenyl)[32a,68] derivatives) only leads to slightly reduced fluorescence quantum yields even in highly viscous solvents. Even a pretwisted 3-Ar group has only a weak influence on the fluorescence quantum yield (the influence of both, pretwisted 1- and 3-substituent is much more pronounced for the spectral band positions).[32a,50,54,68,69] The effect of hydrogen bonding on the fluorescence of the 1,3-diphenyl-Δ^2-pyrazoline chromophore is more pronounced since here only N(2) has a high charge density in the excited state. In the 3-benzothiazol-2-yl-substituted derivatives, dissipation of the negative charge in the N(2)═C(3)−thiazolyl acceptor fragment reduces the charge density at this particular nitrogen atom (cf. section 3.1.4 and the discussion involving protonated **1a**, **1b**, **2a**, and **2b** as well as **3** in sections 3.2.2 and 3.2.3).

Fluorescence Lifetimes. The fluorescence lifetime data are included in Table 2. In apolar solvents, the decay kinetics are always monoexponential. This is also valid for all the derivatives without a 5-*p*-amino donor in all the polar solvents investigated. For the 5-*p*-anilino-substituted derivatives, only in the case of crowned **1c** and **1d**, biexponential decay kinetics with a second, long-lived decay component with a low relative amplitude were found in polar solvents. Global analysis of the fluorescence decay curves recorded as a function of emission wavelength revealed no rise times as well as unchanged relative amplitudes

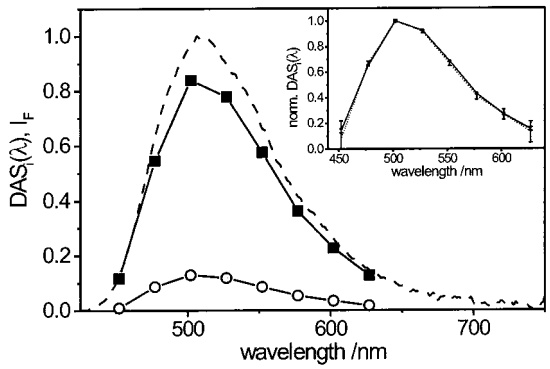

Figure 5. DAS$_i$(λ) (solid lines with symbols) and steady-state emission spectrum (---) of **1d** in acetonitrile at 298 K (excitation at 415 nm, $c_L = 3 \times 10^{-6}$ M). The inset contains the normalized DAS$_i$(λ) with relative errors. Global analysis revealed decay times of 0.98 ns ($\langle a_{rel} \rangle = 0.95$; DAS$_1$($\lambda$) ■, inset —) and 2.96 ns (DAS$_2$(λ) ○, inset ---), respectively.[109]

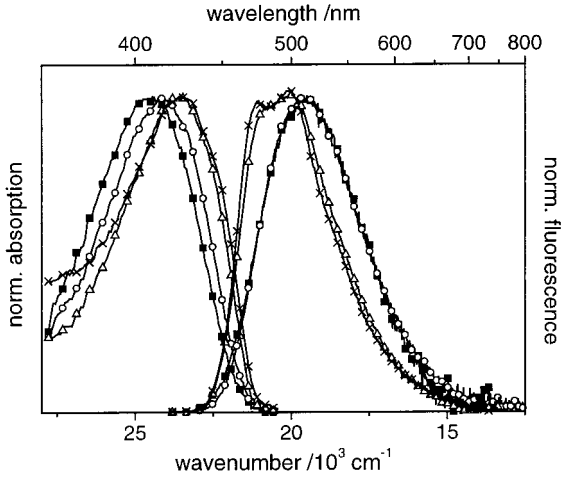

Figure 6. Normalized steady-state absorption and emission spectra of **1a** in ethanol at 290 K (■), 200 K (○), 110 K (△), and 30 K (×).

(<20% for the longer component (3 ns)) over the whole spectral range measured (Figure 5; see eq 1 in section 2.4.). Most probably, this points to the presence of two different emitting conformers in the case of **1c** and **1d**. Assuming similarity of the electronic structure for the crowned derivatives and the parent molecule **1a**, this behavior may arise from conformational flexibility of the aza crown unit (which can induce varying basicity of the amino lone electron pair). Such a conformational flexibility has been recently found by us for the chalcone analogue of **1d**.[17a,49] Keeping in mind the endo−exo isomerization of crown ethers,[70] differences in the interaction between the nitrogen lone electron pair and the 5-phenyl π-system could result in different ET rates and hence different fluorescence decay times. In the case of a tertiary amine "extreme" endo/exo conformations are not possible but an exo conformation with a partly sp^3-hybridized nitrogen atom could alter the rate constant of ET drastically.[71]

3.1.3. Temperature-Dependent Behavior. In order to verify the electron-transfer process in **1a** and its dependence on molecular motions, steady-state and time-resolved fluorescence measurements were carried out with **1a** in ethanol as a function of temperature as well as with **1b**, **2a**, and **2b** in ethanol at 290 and 77 K. As can be seen in Figure 6, the structureless spectroscopic features are maintained within the temperature range of 290−30 K, the spectra at 30 K resembling closely those of **1a** in *n*-hexane (Figure 3). Phosphorescence could not be detected in any of the experiments which means that its quantum yield is less than 0.01[72] and suggests that the remaining 10%

TABLE 5: Spectroscopic Data and Photophysical Properties of 1a, 1b, 2a, and 2b in Ethanol at 290 and 77 K

	T (K)	$\tilde{\nu}$(abs) (10^3 cm^{-1})	$\tilde{\nu}$(em) (10^3 cm^{-1})	$\Delta\tilde{\nu}$(abs−em) (cm^{-1})	ϕ_f	τ_f (ns)	k_f (10^8 s^{-1})	k_{nr} (10^8 s^{-1})
1a	290	24.69	19.51	5180	0.02	0.12	1.7	81.7
1b		24.81	19.45	5360	0.59	3.54	1.7	1.2
2a		27.75	21.27	6480	0.37	3.56	1.0	1.8
2b		27.91	21.37	6540	0.41	3.65	1.1	1.6
1a	77	23.93	20.44	3490	0.85	3.60	2.4	0.4
1b		24.24	20.61	3630	0.87	3.61	2.4	0.4
2a		27.09	23.07	4020	0.97	3.65	2.7	0.1
2b		27.17	23.15	4020	0.97	3.75	2.6	0.1

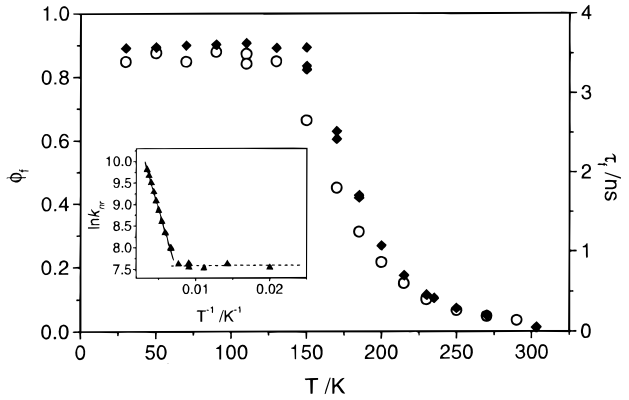

Figure 7. Temperature dependence of the fluorescence quantum yield (○) and lifetime (◆) of **1a** in ethanol. The inset shows the temperature dependence of ln k_{nr} above (—) and below (constant, ---) the glass temperature of ethanol (T_g^{EtOH} = 158 K).

of nonradiative deactivation of **1a** and **1b** are mainly due to internal conversion from S_1 to the ground state. The spectroscopic properties of all the four compounds in ethanol at 290 and 77 K are collected in Table 5. In the case of **1b**, **2a**, and **2b** which are already moderately fluorescent at room temperature, the quenching induced by hydrogen bond formation is suppressed at 77 K and fluorescence quantum yields near unity are observed (Table 5). For all the dyes, monoexponential fluorescence decay kinetics are observed at all the temperatures studied.

Figure 7 combines the corresponding fluorescence quantum yield and lifetime data of **1a**. From a comparison of the kink point in the ϕ_f and τ_f vs T plots for **1a** (Figure 7) with the glass temperature of the solvent (T_g^{EtOH} = 158 K; Figure 7), it is evident that a viscosity-dependent process is frozen below T_g in **1a**. The constant values obtained for both fluorescence quantum yield and lifetime suggest that the quenching ET process is blocked below T_g. The similar data of **1a** and **1b** at 77 K given in Table 5 support these findings.

$$\ln k = \ln A - \frac{E_A}{RT} \tag{8}$$

On the other hand, upon analyzing the temperature-dependent emission data above T_g in terms of the Arrhenius equation (eq 8), a linear correlation is obtained for a plot of ln k_{nr} vs T^{-1}. As a consequence, an activation barrier of 11.3 kJ mol^{-1} is found for the nonradiative processes while k_f does not show a distinct temperature dependence with values of 2 (±0.4) × 10^8 s^{-1} (for **1a**) over the temperature range studied. The temperature dependence of the emission behavior of **1a** in solution points to a mainly viscosity controlled ET process being active only in **1a**.

In order to elucidate whether the viscosity or temperature influence is due to a purely intramolecular relaxation or mainly due to solvent reorientations and to get more insight into the role of hydrogen-bonding interactions, temperature-dependent spectroscopic studies of **1b**−**d** as well as of some of the dyes in polar aprotic solvents are currently performed. If an intramolecular rotation is involved in the ET quenching process, the bulkiness of the 5-*p* substituent in **1c** and **1d** should result in a larger barrier than found here for **1a**.

TABLE 6: Calculated Sum of Bond Angles at N(1) (∑[N(1)]) and Dihedral Angles (θ) of the Molecular Planes of 1a, 1b, 1e, 2a, 2b, 3, and Their Protonated Derivatives in the Ground State[a]

	−R^{+} [b]	∑[N(1)]/deg	θ_{1-2}/deg	θ_{1-3}/deg	θ_{1-4}/deg
1a[c]		347.8	27.4	3.9	87.1
1b[c]		347.6	27.8	3.7	86.5
3[c,d]	N(13)	360.0	20.1	1.6	90.9
1e-H$^+$	N(2)	333.7	87.7	2.6	90.8
1e-H$^+$	N(1)	333.9	90.8	1.6	94.3
2a		346.6	28.9	4.6	86.6
2b		346.4	29.3	5.4	86.2
2b-H$^+$	N(1)	334.0	92.0	1.8	91.9
2b-H$^+$	N(2)	333.5	88.1	2.8	89.8

[a] By AM1/HyperChem; for the definiton of molecular planes, see Table 1. The results obtained for **1c**−**e** and for the protonated species of **1c** and **1d** are similar (±0.5°). [b] Position of protonation or methylation. [c] The anti conformation of N(2) and N(13) is energetically favored (6 kJ mol^{-1}) for **1a**−**e**, but the optimized geometry of the syn conformer shows comparable features. For **3**, the syn conformation of N(2) and N(13)$^+$−CH$_3$ is favored. [d] **1e**−H$^+$/N(13), syn conformation is energetically preferred, shows very similar geometrical parameters as **3** (±0.5°).

3.1.4. Quantum Chemical Calculations. In order to get more insight into the geometric arrangements, charge distribution, and nature of the molecular orbitals involved in the electronic transitions in the 1,3,5-triaryl-Δ^2-pyrazolines, quantum chemical calculations were performed for **1a**−**e**, **2a**, **2b**, **3**, and their protonated derivatives. The latter are important for a better understanding of the complexation experiments (see sections 3.2.1−3.2.3).

Ground-State Geometries. Ground-state geometry optimizations were performed on a semiempirical AM1 level and relevant data of the molecules are summarized in Table 6 (labeling of the atoms according to Scheme 1). A comparison of the X-ray data (molecules in the crystalline state, see Table 1) with the quantum chemical results (molecules in the gas phase, see Table 6) generally yields a good agreement for **1b**, **2a**, and **3**, respectively. The mean deviations in bond lengths are <0.025 Å and the near coplanarity of the 3-substituent and the Δ^2-pyrazoline moiety as well as the anti (or syn) conformation of N(2) and N(13) for **1b** and **2a** (or **3**) are well reproduced by the quantum chemical calculations. Some deviations are found for the degree of pyramidalization at N(1), and the sum of the bond angles at N(24) amount to 350.9° (**1a**), 355.5° (**1c**), 352.6° (**1d**), and 350.6° (**2a**), comparable to those found for **2a** (Table 1) as well as *N*-phenyl-A15C5 and -AT$_4$15C5 in an X-ray structure analysis.[17a,49,71] The dihedral angles between the molecular planes are comparable to values given by Blair et al.

TABLE 7: Calculated Electronic Properties of the Leading Electron Configurations of the ^{1}CT and ^{1}ET States Using ZINDO/S−CI

	config	ΔE_{ACN}[a]/ eV	ΔE_{GAS}/ eV	$\Delta\mu_{eg}$/D	μ_e/D	f	ΔE_{S-T}/ eV
1a	^{1}CT (1→−1)	3.56	3.63	8.3	10	0.91	1.05
	^{1}ET (2→−1)	3.27	4.57	38.3	40	0.006	0.01
2a	^{1}CT (1→−1)	3.86	4.18	15.4	18	0.63	0.94
	^{1}ET (2→−1)	4.03	5.22	31.4	34	0.005	0.007

[a] Calculated from eq 9[45,67] using $\epsilon_S = 37.5$, $n^2 = 1.796$, $a_O = 7.1$ and 6.5 Å, $\mu_g = 1.7$ and 2.6 D for **1a** and **2a**, respectively.

for **2b** (e.g., $\theta_{1-2} = 25.1°$ and $\theta_{1-4} = 93.1°$)[34a] on the basis of AM1/MOPAC calculations[34a] and agree with the X-ray structural data within ±10° (with the exception of θ_{1-2} for **3**, see Tables 1 and 6). Furthermore, the energy barriers for rotation around the sterically unrestricted single bonds are low for all the molecules studied. The activation barriers are calculated to 14.2 and 16.3 kJ mol^{-1} (N(1)−C(6)) and 9.0 and 7.3 kJ mol^{-1} (C(3)−C(12)) for the corresponding single bonds of **1b** and **2b**, respectively. In contrast, rotation around the single bond C(5)−C(18) is connected with a high barrier, i.e., 164 and 159 kJ mol^{-1}, constrained to an almost perpendicular twist angle (~80°) due to the sterical interaction with the neighboring 1-substituent. The protonated and methylated compounds will be discussed further below.

Molecular Orbitals and Differences of CT and ET States. Inspection of the molecular orbitals (MOs) calculated for all the molecules with the AM1 Hamiltonian (Figure S1) reveals that the HOMO−LUMO (1 → −1) transition involves large orbital overlap in the central Δ^2-pyrazoline chromophore which therefore is a strongly allowed transition (cf. Table 7). Since this electron configuration contributes to the S_1 state with more than 90% (from ZINDO/S-CI) and it is also connected with a partial charge transfer from the Δ^2-pyrazoline unit to the almost coplanar substituent in the 3-position, we can assign the corresponding transition to the ^{1}CT state experimentally observed with large fluorescence quantum yields.

In those cases where an anilino group acts as an electron donor in the perpendicularly arranged 5-position (**1a**, **1c**, **1d**, **2a**), the HOMO−1 (MO 2) becomes localized on this donor moiety which consequently leads to the lowest lying electron transfer state associated with full charge separation across the C(5)−C(18) twisted single bond. This explains that only in these compounds a quenching ET state can be expected. The exception of the charged molecule **3** is discussed separately below. To elucidate why this ET process is active only in **1a**, **1c**, and **1d** but not in **2a**, we collected the electronic properties of the leading configuration of the ^{1}ET and ^{1}CT states for **1a** and **2a** in Table 7. As expected for delocalized ^{1}CT states, the oscillator strengths *f* and dipole moments μ_e are relatively large[67] whereas the ^{1}ET transition is forbidden with *f* close to zero and is connected with a giant dipole moment of 40 D for **1a** and 34 D for **2a**. Proof of the radical ion-pair nature of the configuration in question is provided by the near-degeneracy of the singlet and triplet states, revealed in the small singlet−triplet energy gap, or ΔE_{S-T}. In the gas phase (and in apolar solvents), the ^{1}ET state is very high lying but due to the large difference between ground- and excited-state dipole moments ($\Delta\mu_{eg}$) this transition is drastically lowered in solvents such as acetonitrile. In order to estimate this effect, we employed eq 9 with reasonable Onsager parameters.[45,67,73] Indeed, under these conditions the ^{1}ET state becomes lower lying than the ^{1}CT state only for **1a** but not for **2a**, which reflects the experimental observation that ET is not accessible for **2a** in acetonitrile.

TABLE 8: Redox Potentials of 1a−d, 2a, and 2b in Acetonitrile/0.1 M Bu_4NPF_6 vs Fc/Fc^+

	$E_{1/2}$ (ox)/mV		$E_{1/2}$ (red)/mV
1a[a]	440	680	−2220
1a−H$^+$		720	n.d.
1b[a]		590	−2195
1c	470	680	−2210
1d	550[b]	635	−2195
2a	390	570	−2825
2a−H$^+$		490	n.d.
2b		430	−2830

[a] A third oxidation at ca. 1000 mV (**1a**) and 950 mV (**1b**) is found, most probably arising from the benzothiazole moiety. No attempts were made to resolve this peak for **1c** and **1d**. [b] ±20 mV, all others ±5 mV.

The main reason for this effect is the larger value of $\Delta\mu_{eg}$ of ^{1}ET in **1a** and the larger value of $\Delta\mu_{eg}$ of ^{1}CT for **2a** which both result in a stronger stabilization of ^{1}ET against ^{1}CT in **1a** than in **2a**.

$$\Delta E_{Solv} = \Delta E_{GAS} - \frac{1}{a_O^3}\frac{\epsilon_S - 1}{2\epsilon_S + 1}(\mu_e^2 - \mu_e\mu_g) - \frac{1}{a_O^3}\frac{n^2 - 1}{2n^2 + 1}(\mu_e\mu_g - \mu_g^2) \quad (9)$$

When the dimethylanilino donor group is exchanged by a methoxyphenyl group (**1a** → **1e**), the ^{1}ET-induced quenching is not observed because the HOMO of this donor group is lower lying leading to a larger energy gap of the ^{1}ET transition than in the corresponding dimethylanilino derivative. However, a quenching ^{1}ET state is experimentally observed in the charged compound **3** ($\phi_f = 0.07$ in MeCN as compared to $\phi_f = 0.77$ for **1e** in MeCN, see Tables 2 and 12). In this particular case, the calculations predict again a strongly reduced $S_0-{}^1$ET transition energy. In fact, inspection of the atomic charges shows that the positive charge is mainly localized on the BT unit in S_0 while the lowest lying ^{1}ET (S_2 in gas phase) in the excited state results in a charge shift to the methoxyphenyl unit. Such a behavior has recently been explained in a similar way for a pair of uncharged and charged biphenyls, respectively.[74] In the case of a pronounced twist between donor and acceptor unit, the positive charge becomes localized on the acceptor unit, here BT, and enhances its electron affinity, i.e., reducing the ^{1}ET−S_0 energy gap. In addition, the small bond alternation in the excited states of such charged molecules favors a photoinduced conformational relaxation toward a higher twist between both moieties which even supports the previously mentioned effects. As a consequence, the ^{1}ET−S_0 energy gap becomes very small and thus might lead to a conical intersection connected with an efficient nonradiative funnel.[75,76]

3.1.5. Cyclic Voltammetry. For a better understanding of the ET process the redox potentials of **1a**−**d**, **2a**, and **2b** were determined (Table 8). A single reduction is observed at <−2000 mV which is irreversible only in the case of **2b**. The irreversible oxidation of the pyrazoline moiety occurs between 430 mV (for **2b**) and 680 mV (for **1a** and **1c**). For the 5-anilino-substituted compounds, the first oxidation step (390−550 mV) is attributed to an irreversible oxidation of the amino group. Accordingly, this peak is absent in protonated **1a** and **2a**. Introduction of the benzothiazole moiety facilitates the reduction of the dyes by ca. 600 mV but aggravates the oxidation of the amino group by ca. 50 mV and that of the pyrazoline moiety by 60−110 mV. The most striking result of these electrochemical experiments is the comparatively large difference in amino group

oxidation potential observed for **1a**, **1c**, and **1d** differing only in the 5-anilino substituents DMA (**1a**, 440 mV), A15C5 (**1c**, 470 mV), and $AT_4$15C5 (**1d**, 550 mV, Table 8). This order reflects closely the tendencies in ET fluorescence quenching as expressed by fluorescence quantum yields and lifetimes (Table 2).

3.1.6. Intramolecular Electron Transfer. Since the ET quenching process in **1a**, **1c**, and **1d** is absent in **1b**, the rate constant for ET of **1a** in acetonitrile can be calculated from the fluorescence lifetime by using that of **1b** as a reference according to eq 10.[77]

$$k_{et} = \frac{1}{\tau_f^{ET}} - \frac{1}{\tau_f^{ref}} \tag{10}$$

Here, τ_f^{ET-1} is the reciprocal fluorescence lifetime of the molecule with "electron transfer", i.e., **1a** and τ_f^{ref-1} refers to that of the unquenched reference molecule (e.g., $\tau_f^{ref-1} = 2.5 \times 10^8\ s^{-1}$ for **1b** and **1e**), respectively. With the fluorescence lifetime data given in Table 2, the rate constants k_{et} for the ET process in acetonitrile at 298 K are determined to 33, 9, and 0.7 ns^{-1} for **1a**, **1c**, and **1d**, respectively. The rate constants k_{et} are rather small and are not related to the solvent relaxation time[78] which confirms that the rate-determining step of the ET occurs in the nonadiabatic regime. This allows us to characterize the ET reaction in more detail by the following considerations.

The driving force (ΔG_{ET}) for the excited-state electron-transfer reaction (D−A)* → $D^{\bullet+}$−$A^{\bullet-}$ is related to the zero−zero transition energy ΔE_{00} of the precursor (D−A)* state, the donor ionization potential IP_D, the acceptor electron affinity EA_A, and the Coulomb stabilization energy E_C of the radical ion pair $D^{\bullet+}$−$A^{\bullet-}$ by eq 11a (d_{DA} = charge separation distance). IP_D and EA_A can experimentally be determined from the redox potentials $E_{1/2}(D^+/D)$ and $E_{1/2}(A/A^-)$, respectively, according to eqs 12a,b where a relative correction term for the changing charge−solvent stabilization energy in different solvents is considered. The latter is usually approximated by the Born equation for a spherical charge but can in our case be taken as zero, because all parameters are measured and derived for the same solvent (acetronitrile). Hence, eqs 11a and 12a,b combine to the Rehm−Weller expression in eq 11b[79] from which the ET driving forces for some of the investigated Δ^2-pyrazolines, i.e. **1a**, **1e**, and **2a**, in acetonitrile are calculated (Table 9).

$$-\Delta G_{ET} = \Delta E_{00} - IP_D + EA_A + E_C \tag{11a}$$

$$-\Delta G_{ET} = \Delta E_{00} - E_{1/2}(D^+/D) + E_{1/2}(A/A^-) + 2\Delta G_{\pm}^{solv} + \frac{e^2}{\epsilon_s d_{DA}} \tag{11b}$$

$$IP_D = E_{1/2}(D^+/D) - \Delta G_+^{solv} \tag{12a}$$

$$EA_A = E_{1/2}(A/A\text{-}) + \Delta G_-^{solv} \tag{12b}$$

The distinctly more negative ΔG_{ET} value for **1a** is in line with the experimentally obtained results that among the compounds considered in Table 9 the ET takes place only for the 3-benzothiazol-2-yl-substituted 5-*p*-anilino derivative.

Kinetic parameters such as the ET energy barrier $\Delta G^{\#}$ and the solvent reorganization energy can be derived from Marcus ET rate theory employing eqs 13 and 14.[79d,80,81a]

$$\Delta G^{\#} = \frac{\lambda_S}{4}\left(1 + \frac{\Delta G_{ET}}{\lambda_S}\right)^2 - V \tag{13}$$

$$\lambda_S = e^2\left(\frac{1}{2r_{D^+}} + \frac{1}{2r_{A^-}} - \frac{1}{d_{DA}}\right)\left(\frac{1}{n^2} - \frac{1}{\epsilon_S}\right) \tag{14}$$

TABLE 9: Calculated ET Parameters for 1a, 1e, and 2a in Acetonitrile at 298 K

	ΔE_{00} (eV)	$E_{1/2}(D^+/D)$ (eV)	$E_{1/2}(A/A^-)$ (eV)	ΔG^{solv} [a] (eV)	E_C [b] (eV)	ΔG_{ET} [c] (eV)	λ_S [d] (eV)	$\Delta G^{\#} + V$ [e] (cm^{-1})
1a	3.09	0.44	−2.22	0	0.05	−0.48	1.25	960
1e	3.10	1.45 [f]	−2.22	0	0.05	0.52	1.28	5100
2a	3.43	0.39	−2.83	0	0.06	−0.27	1.14	1340

[a] The absolute contribution is included in the measured redox potentials and relative differences are zero for a single solvent. [b] A charge separation distance d_{DA} of 8.3 Å for **1a** and **1e** and 6.6 Å for **2a** as obtained from the core−core distance of the 5-*p*- to the 3-*p*-aryl substituent is used. The dielectric constant of the solvent ϵ_S is 37.5.[c] From eq 11b. [d] From eq 14. [e] From eq 13. [f] Value for methoxybenzene taken from ref 112.

Since no data for the intramolecular reorganization energy (λ_i) are available for our molecules and with the assumption that changes of this type are comparable for both rigid molecules,[82a] λ_i is neglected in eq 13. This simplifaction is reasonable because in highly polar solvents such as acetonitrile λ_i is usually considerably smaller than λ_s (e.g., see ref 81b). V is the electronic coupling matrix element and quantifies electronic interaction between donor and acceptor parts (r_{D^+}, r_{A^-} = ionic radii). In these "pseudo spiro" arranged D−A assemblies, V is not expected to be large. However, weak electronic coupling is known to play a significant role in classical spiro compounds (spiroconjugation)[82b] involving both spiro conjugated π-systems or π-systems and adjacent orbitals with lone electron pairs of heteroatoms such as oxygen or nitrogen. Thus, V cannot be neglected in a process via "pseudo spiro" orientation as for the Δ^2-pyrazolines.

Whereas in the case of **1a** in acetonitrile, $\Delta G^{\#} + V \sim 4.5 k_B T$, the energy barriers in **2a** (ca. $6.5 k_B T$) and in **1e** (ca. $25 k_B T$) are distinctly higher which can further explain why ET occurs only in **1a** (Table 9). Moreover, the reduced ET rate constants in the A15C5 (**1c**) and, more strongly, in the $AT_4$15C5 (**1d**) substituted derivatives are conceivable with the smaller oxidation potentials (Table 8) which yield smaller ΔG_{ET} and larger $\Delta G^{\#}$ than for **1a**. This shows the importance of the exact knowledge of the actual redox potentials of D and A in the case of a "sensitive" ET quenching reaction.[83]

Thus, by tuning the thermodynamic ET properties it is possible to accelerate or slow an excited-state ET process, which can be utilized for sensing activities.

3.2. Complexation Studies. 3.2.1 Complexation Behavior. *Case of **1d**.* The complexation-induced spectroscopic changes of **1d** are strongly dependent on the metal ion (Table 10). Furthermore, as will be discussed in detail below, for metal ions with a strong tendency for chelate formation, complexation to two different coordination sites can occur. However, only complexation to the crown ether moiety is reminiscent of a behavior expected for an "ET analogue" sensing.

Whereas no change in fluorescence quantum yield occurs in the presence of all the alkali and alkaline-earth metal ions, binding to Ag^I (fluorescence enhancement factor FEF = 6.5) and, to a minor extent, Hg^{II} leads to fluorescence enhancement. No effects are observed for the other heavy and transition metal

TABLE 10: Spectroscopic Properties of the Cation Complexes of 1d in Acetonitrile[a]

	$\tilde{\nu}$(abs) (10^3 cm^{-1})	$\tilde{\nu}$(em) (10^3 cm^{-1})	$\Delta\tilde{\nu}_{cp-fp}$(abs)[b] (cm^{-1})	$\Delta\tilde{\nu}_{cp-fp}$(em)[b] (cm^{-1})	ϕ_f	τ_f(blue)[c] (ns)	τ_f(red)[c] (ns)	log K (em, abs)	r_M[d] (Å)	$\chi_m^2 \times r_M$[d,e]
1d[f]	24.94	19.47			0.10	0.98, 2.96[g]				
⊂Hg^{II} [h]	25.13, 21.69	19.61, 16.61	190, −3250	140, −2860	0.22, 0.03	1.23, 2.88[i]	0.59	5.3, 3.6	1.02	4.08
⊂Zn^{II} [j]									0.74	2.01
⊂Cu^{II} [h]	25.06, 21.32 [k]	19.57, 16.60	120, −3620	100, −2870	n.d.	3.2	0.7	n.d.	0.73	2.64
⊂Cu^{I}	24.9	19.5	0	0	0.12	n.d		n.d.	0.96 (4)	3.46
⊂Ag^{I}	25.06	19.61	120	140	0.65	3.70		4.92	1.15	4.28

[a] The experiments were carried out up to the μM concentration range for the heavy and transition metal ions and up to the mM concentration range for the alkali and alkaline-earth metal ions[113] ($c_L = 3 \times 10^{-6}$ M). [b] Cation-induced shifts. [c] "Blue" denotes excitation and emission wavelength set in the high-energy bands, "red" denotes excitation and emission wavelength set in the low-energy bands. [d] All the radii were taken from ref 114a and are for six-coordination except where the coordination number is indicated in parentheses[115a] and for Cu^{I}.[115b] For Cu^{I}, tetrahedral coordination is found in most polythia ether complexes.[116] [e] The electronegativity values given in the literature differ largely in units.[117a] Here, the softness or class B parameter[118] was calculated with the electronegativity values of Allred and Rochow.[117b,c] [f] No effects observed for Li^{I}, Na^{I}, K^{I}, Mg^{II}, Ca^{II}, Sr^{II}, Ba^{II}, and Pb^{II}. [g] $a_{rel}(1) = 0.95$. [h] The low-energy bands are only observed at a metal ion excess of $x_{M/L} > 2$ (upper μM concentration range). Excitation at the high-energy absorption band yields the high-energy emission band and excitation at the low-energy absorption band yields the low-energy emission band. [i] $a_{rel}(1) = 0.85$. [j] A similar behavior is observed for Cd^{II} ($r_M = 0.95$, $\chi_m^2 \times r_M = 2.71$), Ni^{II} (0.69, 2.52), and Co^{II} (0.74, 2.61). [k] For **1d**⊂Cu^{II}, various subbands, exemplified by shoulders in the absorption spectrum were found, whose origin is unclear at present (see text).

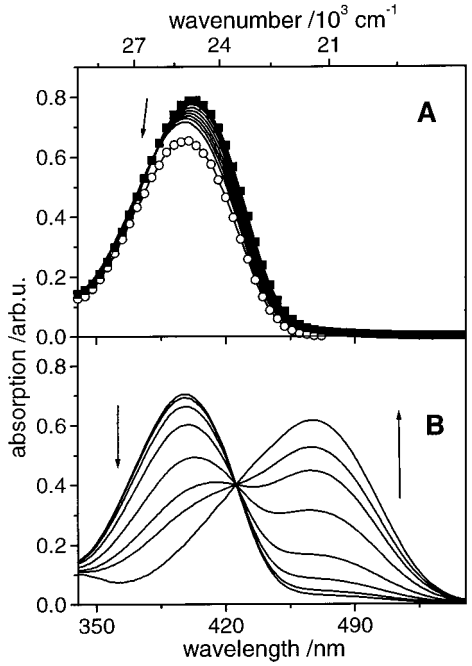

Figure 8. UV/vis spectrophotometric titration spectra of **1d** with Hg^{II} perchlorate in acetonitrile. Hg^{II} addition in the range of $0.02 \le x_{M/L} \le 1$ (A) and $2 \le x_{M/L} \le 100$ (B). The spectrum of uncomplexed **1d** (■) and the absorption spectrum of **1b** (○) are included for better comparison ($c_L = 5 \times 10^{-6}$ M).

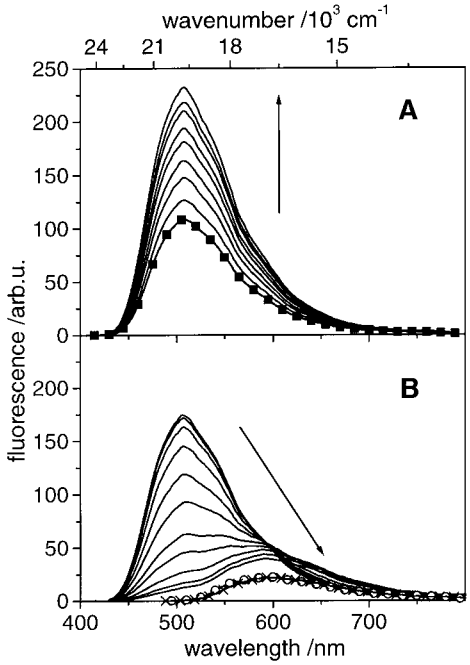

Figure 9. Fluorometric titration spectra of **1d** with Hg^{II} perchlorate in acetonitrile. Hg^{II} addition in the range of $0.02 \le x_{M/L} \le 1$ (excitation at 400 nm, A) and $2 \le x_{M/L} \le 100$ (excitation at isosbestic point 425 nm, B). Solid squares (■) denote the spectrum of uncomplexed **1d**, and the emission spectra of **1d**⊂Hg^{II} at large ion excess excited at 480 nm (○) and of **3** (×) are included for better comparison ($c_L = 1 \times 10^{-6}$ M).

ions (Table 10). For Cu^{II} as well as for Hg^{II}, the appearance of a second red-shifted absorption and emission band is observed at higher cation concentration/excess (metal-to-ligand ratios $x_{M/L} \ge 2$, Figures 8 and 9). For both complexes, excitation at the high-energy absorption band (at ca. 25 000 cm^{-1}) yields the "blue" emission (at ca. 19 600 cm^{-1}) and excitation at ca. 21 600 cm^{-1} gives rise to the red-shifted emission (at ca. 16 600 cm^{-1}). This is in agreement with the observed emission wavelength dependence of the fluorescence excitation spectra and indicates that (at least) two emitting species are present in solution.

A titration of **1d** with Hg^{II} or Cu^{II} yields the following results: For $x_{M/L} < 2$, the absorption band centered at 24 940 cm^{-1} remains nearly unchanged with a slight hypsochromic shift (to ca. 25 100 cm^{-1}) and a decrease of the anilino absorption band at 37 700 cm^{-1} whereas for $x_{M/L} > 2$, a second band located at ca. 21 500 cm^{-1} appears (Figure 8). The corresponding changes in emission are reflected by both fluorescence bands (Figure 9). The absorption and emission spectra at $x_{M/L} = 1$ are identical with the spectra of **1b**, suggesting efficient complexation to the crown ether moiety (Figure 8) yielding a FEF of 2.2. **1d**⊂Cu^{II} shows the same fluorescence features as **1d**⊂Hg^{II} only with reduced fluorescence quantum yields for both emission bands. The origin of the red-shifted bands will be discussed in detail in section 3.2.2.

Similar to the complexation behavior of the chalcone analogue of **1d** toward Cu^{II},[17a] comparably slow kinetics are observed for **1d** and Cu^{II} as well; i.e., the immediately formed complex undergoes a rearrangement, and time-dependent changes in the absorption spectrum are observed.

Whereas the titration spectra for Hg^{II} suggest that complex formation at the two binding sites is consecutive in the case of Cu^{II} (lower complex stability of $AT_4$15C5⊂Cu^{II} as compared to a *N*,*N*-five-membered ring chelate of that ion, see section

TABLE 11: Spectroscopic Properties of the Cation Complexes of 1c in Acetonitrile[a]

	$\tilde{\nu}$(abs) (10^3 cm^{-1})	$\tilde{\nu}$(em) (10^3 cm^{-1})	$\Delta\tilde{\nu}_{cp-fp}$(abs) (cm^{-1})	$\Delta\tilde{\nu}_{cp-fp}$(em) (cm^{-1})	ϕ_f	τ_f (ns)	log K(em)	k_f (10^8 s^{-1})	k_{nr} (10^8 s^{-1})	r_M[b] (Å)	n^2/r_M[b] Z^2 Å^{-1}
1c[c]	25.00	19.52			0.016	0.03[d]		1.5	89		
⊂Li^I	25.06	19.45	60	−70	0.43	2.77	3.00	1.5	2.0	0.76	1.32
⊂Na^I	25.00	19.42	0	−100	0.49	2.88	2.52	1.7	1.8	1.02	0.98
⊂K^I	25.00	19.42	0	−100	(0.21)[e]	2.82	(2.10)[e]	(0.7)	(2.8)	1.46	0.68
⊂Mg^{II}	25.19	19.52	190	0	0.63	4.03	3.16	1.6	0.9	0.72	5.55
⊂Ca^{II}	25.12	19.42	120	−100	0.71	3.99	4.89	1.8	0.7	1.06 (7)	3.77
⊂Sr^{II}	25.06	19.42	60	−100	0.65	3.97	3.87	1.6	0.9	1.21	3.31
⊂Ba^{II}	25.06	19.42	60	−100	0.50	3.98	3.78	1.3	1.3	1.47 (9)	2.72
⊂Pb^{II}	25.19	19.72	190	200	0.54	4.03	5.5	1.3	1.1	1.19	3.36
⊂Hg^{II}, Cu^{II}[f]	21.46	ca. 16.60	−3540	ca. −2920			n.d.	n.d.	n.d.	1.02, 0.73	3.92, 5.48

[a] The experiments were carried out up to the mM concentration range for the alkali and alkaline-earth metal ions and up to the μM concentration range for the heavy and transition metal ions[113] ($c_L = 3 \times 10^{-6}$ M). The corresponding radiative and nonradiative rate constants of **1b** in acetonitrile are 1.8×10^8 s^{-1} (k_f) and 0.7×10^8 s^{-1} (k_{nr}), see Table 3. [b] All the radii were taken from ref 114a and are for six-coordination except where the coordination number is indicated in parentheses.[115a] The values given in parentheses have been found by Jonker in X-ray analyses of related complexes;[115a,c] cavity size of the aza crown: 1.7−1.8 Å.[114b,c] [c] No effects observed for Zn^{II}, Cd^{II}, Ni^{II}, Co^{II}, Cu^{I}, Ag^{I}. [d] Only the main component included. [e] Extrapolated values because full complexation could not be achieved due to solubility problems. [f] These bands are only observed at a metal ion excess of $x_{M/L} > 2$ (upper μM concentration range).

3.2.2) the different kinetics do not allow for a reliable determination of the single fluorescence quantum yields. Thus, a definite statement on the presence or absence of paramagnetic quenching is not possible for Cu^{II}.

The different behavior of Ag^{I}, Hg^{II}, and Cu^{II} is also reflected by the cation-induced changes in fluorescence decay kinetics. Ag^{I} is bound only to the designated receptor part and engages the nitrogen lone electron pair completely in coordination, hence, the fluorescence decay being sufficiently well described by a single-exponential fit (Table 10).

In the presence of Cu^{II}, two decay components are observed. Their relative amplitudes depend on emission and excitation wavelength in the same way as reported before for the corresponding steady-state emission and fluorescence excitation spectra. Here, the longer lifetime of 3.2 ns can be attributed to the "blue" complex with coordination to the crown and the fast decay component of 0.7 ns originates from the "red" chelate (see below for discussion).[84]

For Hg^{II}, the lower FEF as compared to Ag^{I} and the two long-lived decay components with decay times comparable to those of the free probe suggest that the "switching off" of the ET process is either less efficient or counterbalanced by another process. With increasing Hg^{II} concentration, the relative amplitudes remain nearly unchanged ($a_{rel}(1) = 0.85$, Table 10) but a third fast decay component, displaying similar features as the fast component of **1d**⊂Cu^{II}, appears (a_{rel} increases with increasing excitation and detection wavelength). Moreover, the lifetimes of the two slow decay components decrease with increasing Hg^{II} concentration (e.g., from 2.88 ns at $x_{M/L} = 1$ to 2.08 ns at $x_{M/L} = 1000$) pointing to diffusion-controlled fluorescence quenching of this "heavy ion".[15] However, the elucidation of a mechansim accounting for the reduced ET activity of Hg^{II} at $x_{M/L} = 1$ was not possible up to the present stage of investigation. When considering $AT_4$15C5⊂Hg^{II} as a "heavy atom substituent" a possible explanation might arise from the heavy atom effect which has been observed for the 5-*p*-iodo derivative of **2b** before[35a] (although such "heavy atom" interaction was not observed for **1c**⊂Pb^{II}, see below). Other possible explanations involve two ground-state conformers of the complexes showing different ET blocking efficiencies[17a,29,85] or the influence of chelation in the 1,3-chromophore (section 3.2.2).

The higher sensitivity of this ET process as compared to an ICT process is exemplified by complexation of Cu^{I}. Whereas for the chalcone analogue of **1d**, an ICT probe, no spectroscopic changes were detectable upon addition of Cu^{I},[17a] for **1d** a slight but significant fluorescence enhancement is found with Cu^{I}. As would be expected for the complexation site, i.e., the $AT_4$15C5 moiety, and their comparable electronic nature, Cu^{I} behaves very much like Ag^{I} only with less coordinating strength to the nitrogen atom.[86] Moreover, the second evidence for binding of both Ag^{I} and Cu^{I} to the crown ether moiety can be directly concluded from the decrease of the characteristic absorption band of the aniline moiety at 37 700 cm^{-1}.

*Case of **1c**.* In the presence of alkali and alkaline-earth metal ions, the tetraoxa analogue **1c** displays ET sensing properties with analytically favorable average FEFs of ca. 25 for the alkali and ca. 35 for the alkaline-earth metal ions (maximum FEF = 44 for Ca^{II}). These changes in fluorescence quantum yield are reflected by corresponding changes in fluorescence lifetime with the spectral properties remaining nearly unaffected. The spectroscopic properties of the complexes of **1c** are summarized in Table 11. The "switching on/off" nature of the quenching process is further demonstrated by the small differences in fluorescence quantum yields and lifetimes within a group of mono- or divalent main group metal ions. In the complex (full complexation), when the lone electron pair of the anilino nitrogen atom is predominantly engaged in cation binding, the redox properties of the anilino fragment are strongly altered and the ET process is thus blocked.[8] For Ca^{II}, the best fit of ion into the cavity and the high charge density of this cation is demonstrated by identical radiative and nonradiative rate constants of **1c**⊂Ca^{II} and **1b**. Another corollary of electron pair abstraction has been mentioned above and is also found here, the absence of any anilino absorption band for complexed **1c**.

Complete absence of excited-state ET is found in the case of **1c**⊂Pb^{II} as well. Although, Pb^{II} does not fit well into the crown ether's cavity, the ion's "softer" character implies tighter binding to the crown ether nitrogen atom than in the case of the alkaline-earth metal ions. For Cu^{II} and Hg^{II} which should not be complexed to the receptor part of **1c** but can be bound by the 1,3-chromophore, a red-shifted second absorption band was found at higher cation concentrations (Table 11) and led us to a more closer inspection of the nature of the complexes formed.

3.2.2. Nature of the Complexes. Scheme 2 comprises the possible complexation mechanisms of the crowned derivatives **1c** and **1d**. Three different complexes could be formed, i.e., the crown inclusion complex and a bidentate N,N-chelate or S,N-chelate (both with a five-membered ring structure). Since the absorption band of the CT transition in the 1,3-diaryl-Δ^2-pyrazoline chromophore is red-shifted, i.e., the strength of the

SCHEME 2: Possible Coordination Sites in 1,3,5-Triaryl-Δ^2-pyrazolines Containing a Benzothiazolyl Acceptor and a Monoaza Crown Ether Donor. Formation of the Ion−Macrocycle Complex (Route A), a N,N-Chelate (Route B), and a S,N-Chelate (Route C)

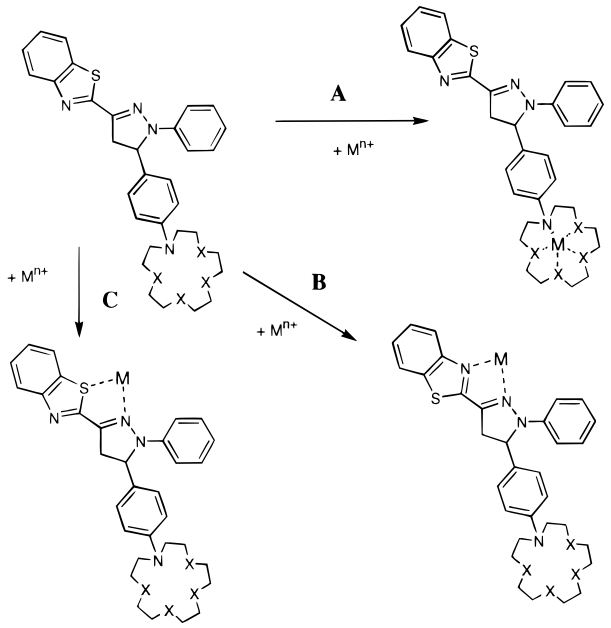

acceptor is increased, complexation to the acceptor part of the 1,3-chromophore is anticipated. To verify the nature of the cation complexes, steady-state absorption and emission measurements were performed with **1a**−**e**, **2a**, **2b**, **3**, and various metal ions.

The absorption spectra of various 3-benzothiazol-2-yl-substituted derivatives in the presence of Hg^{II} (same concentration of dye and $x_{M/L}$) are displayed in Figure 10. Thus, the ability of complex formation to the 5-*p* substituent and chelating site directly correlates to the relative intensities of the bands centered at ca. 25 000 and 21 300 cm^{-1}, respectively. The ratio I_{25000}/I_{21300} decreases on the order of **1d** > **1c** ≈ **1a** > **1b** indicating that only for the $AT_4$15C5 derivative complexation to the macrocyclic moiety occurs whereas for A15C5 and DMA loose coordination to the anilino nitrogen N(24) (without appreciable stabilization by the crown in the case of **1c**) is operative (the anilino band at 37700 cm^{-1} disappears). **1b**, lacking a second coordination site, shows the smallest ratio. A comparison of the band positions of the absorption spectra of the Hg^{II} complexes and **3** shows that interaction of the positively charged ion with the benzothiazole nitrogen atom N(13) and N(2) seems to be responsible for the observed bathochromic shift. Moreover, the emission band of **3** is centered at the same position as the low-energy emission band of the Hg^{II} complexes of the 3-benzothiazol-2-yl-substituted derivatives; see Tables 10−12. As is expected for complexation of a positively charged cation to the acceptor of an ICT chromophore, this "red" complex is stable in the excited state. This is exemplified by the similar Stokes shifts of the chelates of the 3-benzothiazol-2-yl-substituted derivatives and **3** and is reflected by the effects induced upon addition of other heavy and transition metal ions which are not thiophilic (e.g., Zn^{II}). Whereas for **1b** (lacking the anilino nitrogen atom with a high charge density) addition of Zn^{II} leads to the appearance of the red-shifted band, this band is not observed for **1a**/Zn^{II} even at $x_{M/L} = 100$ (a ratio where, e.g., complexation of **1d** to Ag^{I} is complete). Furthermore, loose coordination to the DMA group is exemplified by the observed fluorescence enhancement of the typical emission band of the

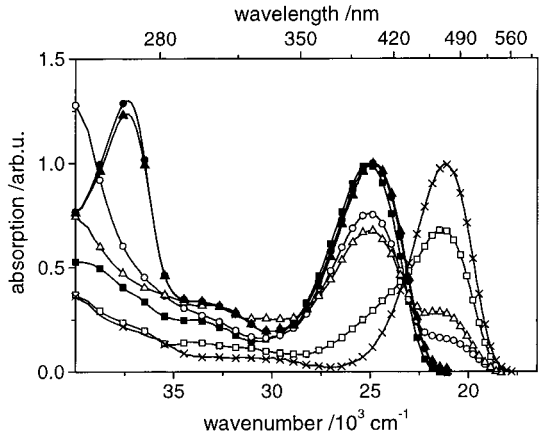

Figure 10. Absorption spectra of **1b** (□, ■), **1c** (△, ▲), and **1d** (○, ●), in the absence (solid signs) and presence (open signs) of an excess of Hg^{II} in acetonitrile ($x_{M/L} = 10$, $c_L = 5 \times 10^{-6}$ M). The spectrum of **3** (×) is included for comparison. The changes in band intensity are directly proportional to the amount of complex formed.

3-benzothiazol-2-yl-substituted derivatives and a decrease in the anilino absorption at 37 700 cm^{-1}. Even for Cu^{II} and **1a**, up to $x_{M/L} \leq 2$, no red-shifted absorption band is measurable.

The protonation studies fit well into this picture. Treating acetonitrile solutions of **1a** and **1b** with 0.01 M $HClO_4$ in acetonitrile leads to the appearance of the intense low-energy absorption band at ca. 21 100 cm^{-1} for both derivatives accompanied by the disappearance of the 37 700 cm^{-1} absorption band in the case of **1a**.[87] Accordingly, excitation in the "red" band produces an emission band centered at ca. 16 600 cm^{-1}, identical to the emission characteristics of **3**. The resulting extraordinary large bathochromic shift observed upon addition of Cu^{II} to a solution of **1b**, i.e., immediate formation of an intense band at 14 000 cm^{-1} (with a shoulder at 15 300 cm^{-1}), will be discussed in a separate paragraph.

Triphenyl-Substituted Derivatives. At first sight, the absence of a new low-energy band upon addition of Hg^{II}, Cu^{II}, Zn^{II}, or any other ion to **2a** or **2b** (for a reaction of **2b** with Cu^{II}, see below) supports the above findings. Regarding only charge density, the ions should be (loosely) coordinated preferably to N(24) and/or N(1) (no chelate formation/stabilization is possible with the 3-substituent of these derivatives) in the ground state and thus, at most, a hypso- instead of a bathochromic shift should occur. But instead, no shifts (besides coordination to N(24) exemplified by a decrease in anilino absorption) are found for both compounds even at a large excess of Zn^{II}, Pb^{II}, Ni^{II}, and Hg^{II}. For **2a**, Cu^{II} induces a hypsochromic shift accompanied by a decrease in molar absorptivity and fluorescence quenching. Whether Cu^{II} coordinates to N(1) (with a higher charge density) or N(2) (sterically more favored) could not be verified. For related heterocycles, i.e., 1-alkylated imidazoles and pyrazoles, the ability of Cu^{II} to bind to the sterically less hindered aromatic nitrogen (without stabilizing chelate formation) is known.[88] Moreover, protonation leads to a similar decrease in the low-energy band of **2a** and **2b** accompanied by an increase of a high-energy band and an isosbestic point at 32150 cm^{-1}. These findings are in accordance with results published by other researchers where protonation (and methylation) takes place at N(1) and excludes the 1-phenyl ring from the chromophore (see $\sum$[N(1)] and θ_{1-2} of **2b**−H^+ in Table 6) leading to a pronounced hypsochromic shift of the absorption band and drastic quenching of the fluorescence.[32a,89]

3.2.3. Quantum Chemical Calculations. Quantum chemical AM1/CI calculations support the findings of the protonation

TABLE 12: Spectroscopic Properties of Various Cation Complexes of 1,3,5-Triaryl-Δ^2-pyrazolines in Acetonitrile[a]

	$\tilde{\nu}$(abs)^{blue} (10^3 cm^{-1})	$\tilde{\nu}$(abs)^{red} (10^3 cm^{-1})	$\tilde{\nu}$(em)^{blue} (10^3 cm^{-1})	$\tilde{\nu}$(em)^{red} (10^3 cm$^{-1)}$	$\Delta\tilde{\nu}_{cp-fp}$(abs)^{red} (cm^{-1})	$\Delta\tilde{\nu}_{cp-fp}$(em)^{red} (cm^{-1})	rel fluor[b]
1d[c]	24.94		19.47				
⊂Hg^{II}	25.13	21.69	19.61	16.61	−3250	−2860	E
1a[d]	24.94		19.34				
⊂Hg^{II} [e]	(24.94)	21.69	(19.34)	16.61	−3250	−2730	(E)
⊂Zn^{II}	(24.94)		(19.34)				(E)
⊂H$^+$ [f]	(24.94)	21.19	(19.34)	16.58	−3750	−2760	(E)
1b[g]	25.13		19.17				
⊂Hg^{II}		21.69		16.61	−3440	−2560	Q
⊂Cu^{II}		14.00, 15.29 (sh)		n.d.	−11130		Q
⊂Zn^{II}		21.74		16.61	−3390	−2560	Q
−H$^+$		21.05		16.58	−4080	−2590	Q
2a[h]	27.70		21.34				
⊂Cu^{II}	(28.17)		(21.34)				(Q)
−H$^+$	39.21				11 510		Q
2b[h]	28.09		21.50				
⊂Cu^{II}		15.06, 16.29 (sh)		n.d.	−13030		Q
−H$^+$	39.21				11 120		Q
3	21.10		16.49				

[a] **3** in MeCN: $\phi_f = 0.07$, $\epsilon[\tilde{\nu}(\text{abs})] = 33.5 \times 10^3$ M^{-1} cm^{-1}; (sh) = shoulder. [b] "E" = enhancement, "Q" = quenching of the blue emission band; letters and values in parentheses refer to effects due to loose coordination to N(24). [c] Similar effects observed for protons and **1a**. [d] Similar effects observed for **1c**. [e] Similar effects for Cu^{II} at $x_{M/L} = 2$, only quenching. [f] Protonation at N(24) and fluorescence enhancement at low concentrations indicated in parentheses. [g] Similar effects are observed for **1e**; (sh) = shoulder, see text. [h] No effects observed in the presence of Zn^{II} and Hg^{II} (only a decrease in anilino absorption for **2a**).

experiments, i.e., only protonation (or methylation as in the case of **3**) at N(13) can explain the observed proton-induced red-shift of the absorption spectra of **1a**−**e** (Table 12). Accordingly, a calculated transition shifted to lower energies with a high oscillator strength is only found for **3** at 22 690 cm^{-1}/$f = 0.87$ and **1e**−H$^+$/N(13) at 22 620 cm^{-1}/$f = 0.89$ (in the gas phase). These values are in good agreement with the experimentally found transitions for **3**, centered at 21 100 cm^{-1} ($f = 0.41$, calculated according to eq 17[90]) in acetonitrile and at 21 280 cm^{-1} in *n*-hexane/1,4-dioxane 2:1, respectively (due to poor solubility, f was not determined in the less polar solvent mixture). For both other possible protonation sites, the calculations predict an antiauxochromic effect (lowest transitions as calculated for the molecule in the gas phase at $\tilde{\nu}$(abs,theo) = 24 570 cm^{-1}, $f = 0.08$ for **1e**−H$^+$ at N(2), and $\tilde{\nu}$(abs,theo) = 27 470 cm^{-1}, $f = 0.21$ for **1e**−H$^+$ at N(1), as well as $\sum$[N(1)] ∼ 333° and $\theta_{1-2} \sim 90°$; Table 6), most pronounced for the nitrogen atom with the highest charge density, N(1). The same tendency is found for the protonated triphenyl-substituted derivatives and is supported by the experimental results, i.e., a strong hypsochromic shift upon protonation.

Although the highest charge density in the ground state is expected to reside at N(1) (the calculations reveal the order of N(24) > N(1) ≥ N(13) ≫ N(2)), delocalization as depicted in Scheme 3 is possible in **1a**−**e** and results in a nearly similar bond order (with pronounced π-character for the single bonds)[47] within the chromophore. This is supported by the fact that the pK_a value of alkyl- or aryl-substituted benzothiazoles is considerably high in acetonitrile.[91] Furthermore, pyramidalization at N(1) is lost (cf. section 3.1.1) and full orbital interaction of sp^2-hybridized N(1) within the remaining chromophore is gained (Table 6).[92] Moreover, coordination to N(13) and N(2) is confirmed by a comparison of the stability constants of the corresponding Cu^{II} complexes with those obtained for a series of substituted pyridines. Here, N,N-chelation of Cu^{II} by 2-pyrid-2-yl-1,3-thiazole yields log $K = 5.65$,[93] whereas this value is much smaller for 5-pyrid-2-yl-1,3-thiazole (log $K = 1.70$),[94] where only stabilization via a S,N-chelate is possible and clearly not favored. Furthermore, the benzothiazole nitrogen donor atom is known to form chelates with transition metal ions in the presence of a second coordination site.[95] Additionally, the

SCHEME 3: Possible Mesomeric Stabilization of a Positive Charge at N(13) (or N(1), Upper Part) and at N(2) (Lower Part)

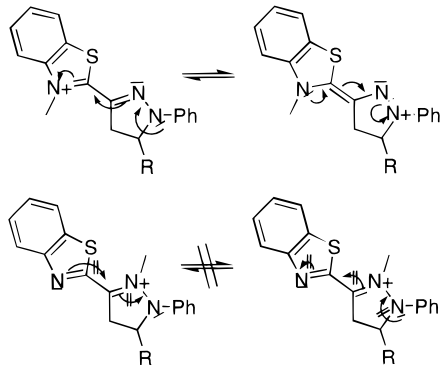

quantum chemical calculations reported above reveal that the charge density is much higher at N(13) than at S(14). Hence, N,N-chelation is anticipated for the acceptor chelates of **1a**−**e**.

The complications imposed on the interpretation of the absorption spectra by Cu^{II} thioether photophysics has recently been discussed for AT$_4$15C5−Cu^{II} interaction.[17a] Similar observations, i.e., partly different absorption spectra for **1d**⊂Cu^{II} compared to that of corresponding **1d**⊂Hg^{II}, were also found here. The large overlap of electronic transitions centered on the fluorescent probe and on the Cu^{II} thioether fragment did not allow for any spectral separation and a further assignment of single bands (see ref 17a for a more detailed discussion).

3.2.4. Reaction of 1b and 2b with Cu^{II}. Already at $x_{M/L} = 1$, the presence of Cu^{II} in an acetonitrile solution containing **1b** or **2b** leads to an immediate change in color from yellow (**1b**) or colorless (**2b**) to deep blue (14 000 cm^{-1} for **1b**, 15 060 cm^{-1} for **2b**, Figure 11). Both spectra are comparable in shape and display a shoulder at the high-energy side (ca. 1300 cm^{-1} shifted to higher energies; the shoulder is more pronounced in the case of **1b**). Furthermore, both bands are more intense than the lowest energy absorption bands of the "uncomplexed" dye.

These results seem to be surprising but can be understood in terms of a simple redox reaction which has been observed before by Pragst et al.[53,96] and which is the basis of the "Knorrsche

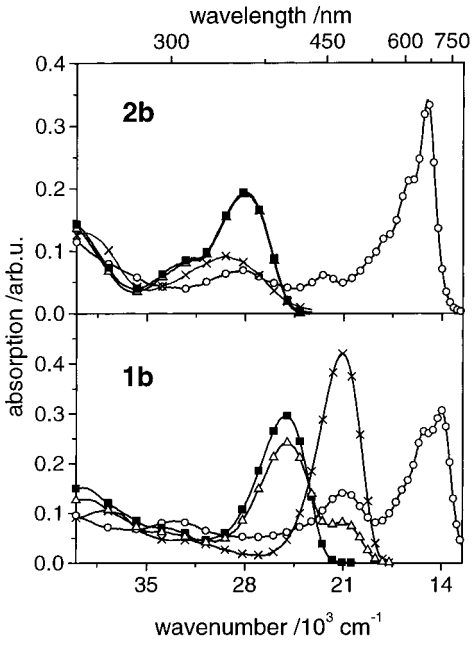

Figure 11. Absorption spectra of **1b** and **2b** in the absence and presence of Cu^{II}, Zn^{II}, and H^+ in acetonitrile. The spectra displayed were recorded for solutions containing the dye (■) and Zn^{II} (△, $x_{M/L}$ = 10, superimposed with ■ for **2b**), Cu^{II} (○, $x_{M/L}$ = 2), or 0.01 M $HClO_4$ (×) ($c_L = 1 \times 10^{-5}$ M).

Pyrazolinprobe" (Knorr's pyrazoline test).[97] The dicationic product of Knorr's test or Pragst's electrochemical oxidation of **2b** shows a similar intense absorption band as the reaction product of **2b** and Cu^{II}.[53,96−98] The dication is a highly planar bis(1-[3-aryl-Δ^2-pyrazolinyl])biphenyl derivative and electron delocalization is possible within the whole chromophore, leading to the structured and intense near-IR absorption.[53] In accordance with Pragst's results, no reaction was observed for **1a** and **2a** in neutral acetonitrile.[96] The oxidizing agent used in Knorr's test is Fe^{III}, but our observations demonstrate that a similar reaction is induced by redox active Cu^{II} in acetonitrile as well. The strong oxidizing power of Cu^{II} in acetonitrile is manifested in the positive half-wave potential $E_{1/2}(Cu^{II}/Cu^{I}) = 0.96$ V vs SCE[99] (as compared to $E_{1/2}(Cu^{II}/Cu^{I}) = -0.09$ V vs SCE in water).[99] Particularly in this solvent, both the amount of stabilizing solvation of Cu^{I} and destabilizing solvation of Cu^{II} account for this pronounced difference. For a better comparison, Figure 11 combines all the metal ion or proton-induced absorption changes found for **1b** and **2b** in acetonitrile.

3.2.5. Some Aspects Toward Analytical Applications. The complex stability constants obtained for **1c** and **1d** agree with the tendencies reported for related fluorescent probes.[17,43b,85,100] The preference of A15C5 for small cations (unless they are not too small like, e.g., Mg^{II}) with a high charge density is demonstrated by the order of complex stability constants, i.e., $Ca^{II} \gg Sr^{II} > Ba^{II} > Mg^{II} > Li^{I} \gg Na^{I} > K^{I}$. Whereas the sensing potential of these ET probes is higher (due to larger FEFs) as compared to ICT probes, this increase in sensitivity is accompanied by a lack in specificity. For example, in the case of **1c**, all the alkaline-earth and alkali metal cations yield similar fluorescence lifetimes and comparable FEFs, rendering it impossible to spectroscopically discriminate between different mono- or divalent cations. Upon exchanging the macrocyclic receptor, similar ion binding preferences are found as in the case of their chalcone analogue fluorescent probes.[17]

The high FEFs observed for the alkali and alkaline-earth metal ions and **1c** suggest that the latter can act as a suitable sensor

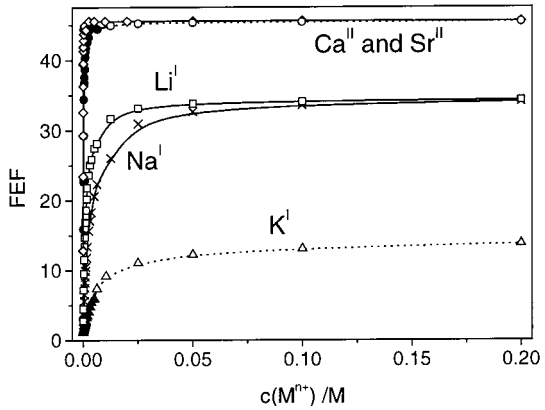

Figure 12. Plot of FEF vs metal ion concentration for **1c** and Ca^{II} (◇), Sr^{II} (●), Li^{I} (□), Na^{I} (×), and K^{I} (▲) in acetonitrile ($c_L = 1 \times 10^{-6}$ M). Because of the limited solubility of Sr^{II} and K^{I} perchlorates in acetonitrile, the data at high cation concentrations are extrapolated (---) and include some points of support (○, △).

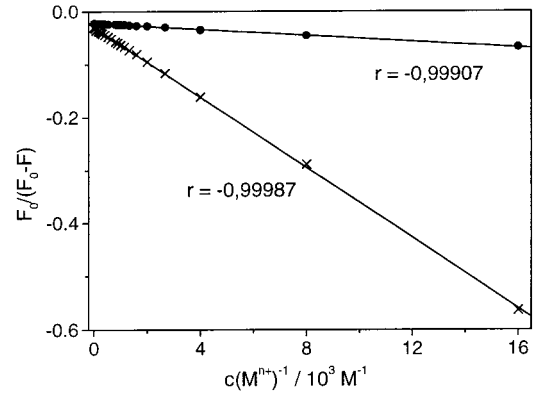

Figure 13. Fit of a $F_0/(F_0 - F)$ vs c_M^{-1} plot for **1c** and titrations with Sr^{II} (●) and Na^{I} (×) in acetonitrile ($c_L = 1 \times 10^{-6}$ M).

molecule for these ions in the micromolar to millimolar concentration range in solution (Figure 12).[101] Especially valuable is the insensitivity of the main fluorophore toward binding of Pb^{II} to the 5-receptor, i.e., large FEF without pronounced "heavy ion" interaction. The excellent correlation observed for a plot of metal ion concentration vs fluorescence intensity is indicated in Figure 13 and suggests a straightforward applicability in chemical analysis. In the case of Ag^{I}, application of **1d** is favorable when excluding (masking) Cu^{II} and Hg^{II}. Similarly, given the absence of Ag^{I} and Cu^{II}, **1d** could be employed for sensing Hg^{II}. Moreover, the interference of oxidizing metal ions such as Cu^{II} is strongly reduced in protic solvents such as alcohols ($E_{1/2}(Cu^{II}/Cu^{I}) = 0.26$ V vs SCE in ethanol)[99] and water since Cu^{II} is more stabilized in these solvents.

Compared to other ET fluorescent probes, the FEFs obtained for **1c** are promising. While gaining a bathochromic shift of 30−50 nm, the sensing potential should at least be equal to that of other Δ^2-pyrazoline ET probes recently introduced by de Silva et al. (their investigations were carried out in methanol).[2a,102] Higher FEFs (see refs 22, 24, 29, 85, and 103) might be possible but the increase in ET efficiency with increasing strength of the 3-acceptor, and hence an increasing ICT in the 1,3-chromophore is always counterbalanced by the smaller energy gap between excited and ground state for the latter process according to the energy gap rule.[104]

Another aspect which needs careful consideration for future probe design is obviously acceptor complexation. Although, in the present case, the FEF observed for **1d** and Hg^{II} are

comparatively small for ET probes, the dynamic working range for metal ion sensing is largely extended compared to probes with a single complexation site. Such bifunctional probes are of special interest for devices with "logic" functions.[2]

4. Conclusion

This quantitative study comprises a detailed photophysical characterization of intramolecular electron-transfer processes in a series of donor−Δ^2-pyrazoline−acceptor compounds with and without cation receptor units and an analysis of their usefulness for applications as metal ion-sensitive fluorescent probes.

All the compounds undergo a partial charge transfer or charge shift in the case of the charged compounds directly after excitation connected with a large oscillator strength and a change of the dipole moment. The spectral and radiative properties of this process can be modified if metal ions are complexed at a receptor unit (5-*p*-crown or 3-Ar chelate). However, improved probe characteristics can only be achieved in those compounds where an electron transfer across the central pyrazoline ("pseudo spiro" spacer) unit occurs. By modifying the ionization potential or electron affinity of the donor or acceptor, respectively, some molecules have been designed to introduce a highly efficient quenching electron-transfer channel with rate constants of 1−30 ns^{-1} in the case of negative driving forces that can be "switched off" in the presence of alkali, alkaline-earth as well as heavy and transition metal cations, these features being especially of analytical importance for the latter ions.

In conclusion, the present studies of the 1,5-diphenyl-3-benzothiazol-2-yl-substituted Δ^2-pyrazolines reveal the sensitivity of intramolecular CT and ET processes on the careful choice of electron donating or accepting substituents in ET signaling systems with short and rigid spacers and demonstrate that the combination of photophysical and electrochemical characterization of model compounds together with quantum chemical calculations allows to perform rational probe design.

Acknowledgment. Financial support by the Deutsche Forschungsgemeinschaft (DFG: Re 387/8-2) and the Bundesministerium für Bildung und Forschung (BMBF, 13N7120) is gratefully acknowledged. The authors thank Dr. M. Kollmannsberger, University of Regensburg, for the electrochemical measurements and M. Spieles for technical assistance.

Supporting Information Available: Syntheses, analytical data, details on metal perchlorate treatment, and X-ray crystallographic data including 12 tables and one figure. This material is available free of charge via the Internet at http://pubs.acs.org.

References and Notes

(1) Fabbrizzi, L.; Poggi, A. *Chem. Soc. Rev.* **1995**, 197. de Silva, A. P.; Gunaratne, H. Q. N.; Gunnlaugsson, T.; Huxley, A. J. M.; McCoy, C. P.; Rademacher, J. T.; Rice, T. E. *Adv. Supramol. Chem.* **1997**, *4*, 1. de Silva, A. P.; Huxley, A. J. M. In *Applied Fluorescence in Chemistry, Biology, and Medicine*; Rettig, W., Strehmel, B., Schrader, S., Seifert, H., Eds.; Springer: Berlin, 1999; p 179.

(2) (a) de Silva, A. P.; Gunaratne, H. Q. N.; Maguire, G. E. M. *J. Chem. Soc., Chem. Commun.* **1994**, 1213. (b) Credi, A.; Balzani, V.; Langford, S. J.; Stoddart, J. F. *J. Am. Chem. Soc.* **1997**, *119*, 2679. (c) de Silva, A. P.; Gunaratne, H. Q. N.; McCoy, C. P. *J. Am. Chem. Soc.* **1997**, *119*, 7891. (d) de Silva, A. P.; Dixon, I. M.; Gunaratne, H. Q. N.; Gunnlaugsson, T.; Maxwell, P. R. S.; Rice, T. E. *J. Am. Chem. Soc.* **1999**, *121*, 1393.

(3) Heitele, H.; Michel-Beyerle, M. E. *J. Am. Chem. Soc.* **1985**, *107*, 8286. Wasielewski, M. R.; Minsek, D. W.; Niemczyk, M. P.; Svec, W. A.; Yang, N.-C. C. *J. Am. Chem. Soc.* **1990**, *112*, 2823. Lewis, F. D.; Burch, E. L. *J. Phys. Chem.* **1996**, *100*, 4055. Higashida, S.; Tsue, H.; Sugiura, K.; Kaneda, T.; Sakata, Y.; Tanaka, Y.; Taniguchi, S.; Okada, T. *Bull. Chem. Soc. Jpn.* **1996**, *69*, 1329. Aviram, A. *J. Am. Chem. Soc.* **1988**, *110*, 5687. Herz, T.; Gedeck, P.; Clark, T. *J. Am. Chem. Soc.* **1999**, *121*, 1379. Jones, G., II; Lu, L. N.; Fu, H.; Farahat, C. W.; Oh, C.; Greenfield, C. R.; Gosztola, D. J.; Wasielewski, M. R. *J. Phys. Chem. B* **1999**, *103*, 572. Pullen, S. H.; Edington, M. D.; Studer-Martinez, S. L.; Simon, J. D.; Staab, H. A. *J. Phys. Chem. A* **1999**, *103*, 2740. Piotrowiak, P. *Chem. Soc. Rev.* **1999**, 143.

(4) Lauteslager, X. Y.; van Stokkum, I. H. M.; van Ramesdonk, H. J.; Brouwer, A. M.; Verhoeven, J. W. *J. Phys. Chem. A* **1999**, *103*, 653. Ji, H.-F.; Dabestani, R.; Brown, G. M.; Hettich, R. L. *Photochem. Photobiol.* **1999**, *69*, 513.

(5) Warman, J. M.; Smit, K. J.; Jonker, S. A.; Verhoeven, J. W.; Oevering, H.; Kroon, J.; Paddon-Row, M. N.; Oliver, A. M. *Chem. Phys.* **1993**, *170*, 359. Verhoeven, J. W.; Scherer, T.; Wegewijs, B.; Hermant, R. M.; Jortner, J.; Bixon, M.; Depaemelaere, S.; De Schryver, F. C. *Recl. Trav. Chim. Pays-Bas* **1995**, *114*, 443.

(6) Cortés, J.; Heitele, H.; Jortner, J. *J. Phys. Chem.* **1994**, *98*, 2527.

(7) Marcus, R. A.; Sutin, N. *Biochim. Biophys. Acta* **1985**, *811*, 265. Brunschwig, B. S.; Sutin, N. *Coord. Chem. Rev.* **1999**, *187*, 233.

(8) Bissell, R. A.; de Silva, A. P.; Gunaratne, H. Q. N.; Lynch, P. L. M.; Maguire, G. E. M.; Sandanayake, K. R. A. S. *Chem. Soc. Rev.* **1992**, 187. Bissell, R. A.; de Silva, A. P.; Gunaratne, H. Q. N.; Lynch, P. L. M.; Maguire, G. E. M.; McCoy, C. P.; Sandanayake, K. R. A. S. *Top. Curr. Chem.* **1993**, *168*, 223.

(9) Czarnik, A. W. *Acc. Chem. Res.* **1994**, *27*, 302.

(10) Valeur, B. In *Probe Design and Chemical Sensing*; Lakowicz, J. R., Ed.; Plenum: New York, 1994; p 21.

(11) Rettig, W.; Lapouyade, R. In *Probe Design and Chemical Sensing*; Lakowicz, J. R., Ed.; Plenum: New York, 1994; p 109.

(12) de Silva, A. P.; Gunaratne, H. Q. N.; McCoy, C. P. *J. Am. Chem. Soc.* **1997**, *119*, 7891.

(13) Rurack, K.; Bricks, J. L.; Kachkovskii, A. D.; Resch, U. *J. Fluoresc.* **1997**, *7*, 63S.

(14) de Silva, A. P.; Gunaratne, H. Q. N.; Gunnlaugsson, T.; Huxley, A. J. M.; McCoy, C. P.; Rademacher, J. T.; Rice, T. E. *Chem. Rev.* **1997**, *97*, 1515.

(15) McClure, D. S. *J. Chem. Phys.* **1952**, *20*, 682. Robinson, G. W. *J. Chem. Phys.* **1967**, *46*, 572.

(16) Varnes, A. W.; Dodson, R. B.; Wehry, E. L. *J. Am. Chem. Soc.* **1972**, *94*, 946. Masuhara, H.; Shioyama, H.; Saito, T.; Hamada, K.; Yasoshima, S.; Mataga, N. *J. Phys. Chem.* **1984**, *88*, 5868. Banfield, T. L.; Husain, D. *Trans. Faraday Soc.* **1969**, *65*, 1985.

(17) (a) Rurack, K.; Bricks, J. L.; Reck, G.; Radeglia, R.; Resch-Genger, U. *J. Phys. Chem. A* **2000**, *104*, 3087. (b) Rurack, K.; Bricks, J. L.; Slominskii, J. L.; Resch-Genger, U. In *Near-Infrared Dyes for High Technology Applications*; Dähne, S., Resch-Genger, U., Wolfbeis, O. S., Eds.; Kluwer Academic: Dordrecht, 1998; p 191.

(18) Ishikawa, J.; Sakamoto, H.; Mizuno, T.; Otomo, M. *Bull. Chem. Soc. Jpn.* **1995**, *68*, 3071. Ishikawa, J.; Sakamoto, H.; Wada, H. *J. Chem. Soc., Perkin Trans. 2* **1999**, 1273.

(19) Lindoy, L. F. In *Cation Binding by Macrocycles*; Inoue, Y., Gokel, G. W., Eds.; Marcel Dekker: New York, 1990; p 599.

(20) Pearson, R. G. *J. Am. Chem. Soc.* **1963**, *85*, 3533. Pearson, R. G. *Inorg. Chem.* **1988**, *27*, 734.

(21) Clarke, R. J.; Coates, J. H.; Lincoln, S. E. *Inorg. Chim. Acta* **1988**, *153*, 21.

(22) Akkaya, E. U.; Huston, M. E.; Czarnik, A. W. *J. Am. Chem. Soc.* **1990**, *112*, 3590. Chae, M.-Y.; Cherian, X. M.; Czarnik, A. W. *J. Org. Chem.* **1993**, *58*, 5797.

(23) Fabbrizzi, L.; Licchelli, M.; Pallavicini, P.; Perotti, A.; Taglietti, A.; Sacchi, D. *Chem. Eur. J.* **1996**, *2*, 75. De Santis, G.; Fabbrizzi, L.; Licchelli, M.; Mangano, C.; Sacchi, D.; Sardone, N. *Inorg. Chim. Acta* **1997**, *257*, 69.

(24) Ghosh, P.; Bharadwaj, P. K.; Mandal, S.; Ghosh, S. *J. Am. Chem. Soc.* **1996**, *118*, 1553.

(25) Sclafani, J. A.; Maranto, M. T.; Sisk, T. M.; Van Arman, S. A. *Tetrahedron Lett.* **1996**, *37*, 2193.

(26) Klonkowski, A. M.; Kledzik, K.; Ossowski, T.; Jankowska-Frydel, A. *J. Mater. Chem.* **1998**, *8*, 1245.

(27) Ramachandram, B.; Samanta, A. *Chem. Phys. Lett.* **1998**, *290*, 9. Ramachandram, B.; Samanta, A. *J. Phys. Chem. A* **1998**, *102*, 10579.

(28) Hennrich, G.; Sonnenschein, H.; Resch-Genger, U. *J. Am. Chem. Soc.* **1999**, *121*, 5073.

(29) Rurack, K.; Kollmannsberger, M.; Resch-Genger, U.; Daub, J. *J. Am. Chem. Soc.* **2000**, *122*, 968.

(30) They are widely used as whitening or brightening reagents for paper, textile fibres, and plastics[105a−c] as well as wavelength shifters in scintillation counting.[68,105d−f]

(31) Kutsyna, L. M.; Voevoda, L. V.; Tishchenko, V. G.; Shepel, A. V. *Opt. Spectrosc.* **1969**, *26*, 91.

(32) (a) Strähle, H.; Seitz, W.; Güsten, H. *Ber. Bunsen-Ges. Phys. Chem.* **1976**, *80*, 288. (b) Strähle, H.; Seitz, W.; Güsten, H. *Z. Naturforsch.* **1976**, *31b*, 1248. (c) Güsten, H.; Heinrich, G.; Frühbeis, H. *Ber. Bunsen-Ges. Phys. Chem.* **1977**, *81*, 810.

(33) (a) de Costa, M. D. P.; de Silva, A. P.; Pathirana, S. T. *Can. J. Chem.* **1987**, *65*, 1416. (b) de Silva, A. P.; Gunaratne, H. Q. N.; Lynch, P. L. M. *J. Chem. Soc., Perkin Trans. 2* **1995**, 685.

(34) (a) Blair, J. T.; Sahyun, M. R. V.; Sharma, D. K. *J. Photochem. Photobiol., A Chem.* **1994**, *77*, 133. (b) Sahyun, M. R. V.; Crooks, G. P.; Sharma, D. K. *Proc. SPIE-Int. Soc. Opt. Eng.* **1991**, *1436*, 125.

(35) (a) Rivett, D. E.; Rosevear, J.; Wilshire, J. F. K. *Aust. J. Chem.* **1979**, *32*, 1601. (b) Rivett, D. E.; Rosevear, J.; Wilshire, J. F. K. *Aust. J. Chem.* **1983**, *36*, 1649. (c) Leaver, I. H.; Rivett, D. E. *Mol. Photochem.* **1974**, *6*, 113.

(36) (a) Yan, Z.-L.; Wu, S.-K. *Ganguang Kexue Yu Guang Huaxue* **1994**, *12*, 80. (b) Yan, Z.-L.; Wu, S.-K. *Ganguang Kexue Yu Kuang Huaxue* **1993**, *11*, 14.

(37) de Silva, A. P.; Gunaratne, H. Q. N.; Gunnlaugsson, T.; Nieuwenhuizen, M. *Chem. Commun. (Cambridge)* **1996**, 1967.

(38) *Gmelins Handbuch der Anorganischen Chemie. Chlor*, 8th ed.; VCH: Berlin, 1927.

(39) (a) Olmsted, J., III *J. Phys. Chem.* **1979**, *83*, 2581. (b) Drexhage, K. H. *J. Res. Natl. Bur. Stand.* **1976**, *80A*, 421.

(40) Resch, U.; Rurack, K. *Proc. SPIE-Int. Soc. Opt. Eng.* **1997**, *3105*, 96.

(41) (a) Boens, N.; Tamai, N.; Yamazaki, I.; Yamazaki, T. *Photochem. Photobiol.* **1990**, *52*, 911. (b) Eaton, D. F. *Pure Appl. Chem.* **1988**, *60*, 1107. (c) Velapoldi, R. A.; Epstein, M. S. In *Luminescence Applications in Biological, Chemical, Environmental, and Hydrological Sciences*; Goldberg, M. C., Ed.; ACS Symp. Ser. Vol. 383, American Chemical Society: Washington, DC, 1989; p 98.

(42) Löfroth, J.-E. *Anal. Instrum.* **1985**, *14*, 403. Löfroth, J.-E. *J. Phys. Chem.* **1986**, *90*, 1160. Beechem, J. M. *Methods Enzymol.* **1992**, *210*, 37.

(43) (a) Bourson, J.; Pouget, J.; Valeur, B. *J. Phys. Chem.* **1993**, *97*, 4552. (b) Fery-Forgues, S.; Le Bris, M. T.; Guetté, J.-P.; Valeur, B. *J. Phys. Chem.* **1988**, *92*, 6233.

(44) Dewar, M. J. S.; Zoeblich, E. G.; Healy, E. F.; Stewart, J. P. P. *J. Am. Chem. Soc.* **1985**, *107*, 3202.

(45) Zerner, M. C.; Karelson, M. M. *J. Phys. Chem.* **1992**, *96*, 6949.

(46) The X-ray structure data of the compounds investigated have been deposited at the Cambridge Crystallographic Data Centre, 12 Union Road, Cambridge, CB2 1EZ, UK, and the three compounds have been allocated the deposition numbers CCDC 133652 (**1b**), CCDC 133653 (**2a**), and CCDC 133654 (**3**). The crystallographic data are provided in Supporting Information, section S3.

(47) Wheatley, P. J. *Acta Crystallogr.* **1955**, *8*, 224.

(48) Duffin, B. *Acta Crystallogr.* **1968**, *B24*, 1256.

(49) The crystal structures of the compounds referred to in the text (see ref 17a) have been deposited at the Cambridge Crystallographic Data Centre (CCDC): *N*-phenyl-A15C5 (CDCC 132993), *N*-phenyl-$AT_4$15C5 (CDCC 132991), chalcone analogue of **1d** (CCDC 132990).

(50) Buryakovskaya, E. G.; Tsukerman, S. V.; Lavrushin, V. F. *Russ. J. Phys. Chem.* (*Engl. Transl.*) **1975**, *49*, 532.

(51) Pragst, F.; Weber, F. G. *J. Prakt. Chem.* **1976**, *318*, 51.

(52) Nurmukhametov, R. N.; Tishchenko, V. B. *Opt. Spectrosc.* **1967**, *23*, 43.

(53) Pragst, F. *J. Prakt. Chem.* **1973**, *315*, 549.

(54) Yang, G.; Wu, S. *J. Photochem. Photobiol., A Chem.* **1992**, *66*, 69.

(55) Doroshenko, A. O.; Skripkina, V. T.; Schershukov, V. M.; Ponomaryov, O. A. *J. Fluoresc.* **1997**, *7*, 131.

(56) Birks, J. B. *Photophysics of Aromatic Molecules*; Wiley-Interscience: New York, 1970.

(57) The transition energy is an inadequate parameter since both, changes in the twist angle and changes in solvation sphere affect this parameter.

(58) Strähle et al. observed a slightly different solvatochromic behavior for the (substituted) 1,3-diphenyl-Δ^2-pyrazolines, i.e., adoption of a planar structure in the excited state.[32a] Such a conformation is less favored in the triaryl analogues since it requires cooperative rotation of the 5-substituent to avoid steric crowding. Furthermore, quantum chemical calculations reveal higher energy barriers for rotation around Ar−C(3) and N(1)−Ar in the case of **1b** (9.0 and 14.2 kJ mol^{-1}) than in the case of 1-phenyl-3-benzothiazol-2-yl-Δ^2-pyrazoline (2.8 and 11.3 kJ mol^{-1}).

(59) (a) Lippert, E. *Z. Naturforsch.* **1955**, *10a*, 541. (b) Lippert, E. *Z. Elektrochem.* **1957**, *61*, 962. (c) Mataga, N.; Kaifu, Y.; Koizumi, M. *Bull. Chem. Soc. Jpn.* **1956**, *29*, 465.

(60) A crucial point in the determination of ($\mu_e-\mu_g$) is the choice of an appropriate Onsager (solvent cavity) radius. Different methods have been described in the literature involving, e.g., X-ray data[106] or molecular modeling geometries[107] and applying further assumptions suggested, e.g., by Lippert.[59a,b] Here, the method proposed by Edward (on the basis of X-ray data) is used.[106]

(61) The solvent-dependent shifts in absorption observed for the 1,3,5-triaryl-Δ^2-pyrazolines investigated here are much smaller compared to those in emission. Since no experimentally obtained values were accessible, the values used for μ_g were obtained from the optimized geometry in the ground state by semiempirical calculations (AM1).

(62) Contributions of a solvent-induced dipole moment could account for deviations[107] and thus for the analysis of the solvatochromic data, the polarizability of the solute can be taken into account as well[108] resulting in a modified Lippert−Mataga eq 15.

$$\tilde{\nu}(\mathrm{em}) = \tilde{\nu}^{\mathrm{vac}}(\mathrm{em}) + \frac{2\mu_e(\mu_e-\mu_g)}{hc_0a_O^{\ 3}}\left(f'(\epsilon_r)-\frac{1}{2}f'(n)\right) \qquad (15)$$

with

$$f'(\epsilon_r) = \frac{\epsilon_r-1}{\epsilon_r+2}; \quad f'(n) = \frac{n^2-1}{n^2+2} \qquad (16)$$

(63) Catalán, J.; López, V.; Pérez, P.; Martín-Villamil, R.; Rodríguez, J.-G. *Liebigs Ann.* **1995**, 241. Catalán, J. *J. Org. Chem.* **1995**, *60*, 8315.

(64) Bakhshiev, N. G. *Opt. Spectrosc.* **1962**, *13*, 24. Bakhshiev, N. G. *Opt. Spectrosc.* **1962**, *13*, 104.

(65) Bilot, L.; Kawski, A. *Z. Naturforsch.* **1962**, *17a*, 621. Kawski, A. *Acta Phys. Polon.* **1966**, *29*, 507. Their formalism takes into account the polarizability of the solute as well yielding nearly similar results as eq 15.[62]

(66) Shizuka, H. *Acc. Chem. Res.* **1985**, *18*, 141. Herbich, J.; Grabowski, Z. R.; Wójtowicz, H.; Golankiewicz, K. *J. Phys. Chem.* **1989**, *93*, 3439. Herbich, J.; Waluk, J. *Chem. Phys.* **1994**, *188*, 247.

(67) Maus, M.; Rettig, W.; Bonafoux, D.; Lapouyade, R. *J. Phys. Chem. A* **1999**, *103*, 3388.

(68) Güsten, H.; Schuster, P.; Seitz, W. *J. Phys. Chem.* **1978**, *82*, 459.

(69) Güsten, H.; Meisner, R. *J. Photochem.* **1983**, *21*, 53.

(70) Buschmann, H.-J. In *Stereochemical and Stereophysical Behavior of Macrocycles*; Bernal, I., Ed.; Elsevier: Amsterdam, 1987; p 103. In the classical endo conformation, i.e., in unsubstituted A15C5 with a secondary amino nitrogen, the lone electron pair is directed into the crown's cavity and in the exo conformation away from the crown's cavity.

(71) For the two conformers of the chalcone analogue of **1d**, the sum of the bond angles at the crown ether nitrogen atom equals 359.6° and 357.3° in the crystalline state.[17a,49]

(72) Moreover, for **1a** and **1b** in ethanol, no phosphorescence at 77 K could be detected in the spectral region of 430−900 nm and at various delay times in the range of 0.05−100 ms employing the Perkin-Elmer LS50B spectrometer with low-temperature luminescence accessory, flash lamp excitation (fwhm < 10 μs), and gated PMT (the same is found for the reference compound **2a** between 370 and 900 nm). These results were confirmed by measurements of fluorescence polarization in ethanol at 77 K (Spectronics Instruments 8100 fluorometer, He cryostat) according to the method of photoselection (Albrecht, A. C. *J. Mol. Spectrosc.* **1961**, *6*, 84) which allows to discriminate between (overlapping) transitions of different nature (see, e.g., Gudipati, M. S.; Maus, M.; Daverkausen, J.; Hohlneicher, G. *Chem. Phys.* **1995**, *192*, 37). For all four compounds, the degree of anisotropy is constant (±0.05) over the whole range of the emission spectrum (440−650 nm, **1a** and **1b**; 380−560 nm, **2a**).

(73) Onsager, L. *J. Am. Chem. Soc.* **1936**, *58*, 1486.

(74) Rettig, W.; Kharlanov, V. A.; Maus, M. *Chem. Phys. Lett.* **2000**, *318*, 173.

(75) Herzberg, G.; Longuet-Higgins, H. C. *Discuss. Faraday Soc.* **1963**, *35*, 77. Bernardi, F.; Olivucci, M.; Robb, M. A. *Chem. Soc. Rev.* **1996**, 321.

(76) Michl, J.; Bonacic-Koutecký, V. *Electronic Aspects of Organic Photochemistry*; J. Wiley & Sons: New York, 1990.

(77) This simplification is justified by nearly identical radiative rate constants for all 3-benzothiazol-2-yl-substituted derivatives and nonradiative rate constants for **1b** and **1e** in any given solvent.

(78) The longitudinal solvent relaxation time in acetonitrile equals 0.2 ps (Kahlow, M. A.; Kang, T. J.; Barbara, P. F. *J. Phys. Chem.* **1987**, *91*, 6452. Rossky, P. J.; Simon, J. D. *Nature* **1994**, *370*, 263).

(79) (a) Rehm, D.; Weller, A. *Ber. Bunsen-Ges. Phys. Chem.* **1969**, *73*, 834. (b) Rehm, D.; Weller, A. *Isr. J. Chem.* **1970**, *8*, 259. (c) Weller, A. *Z. Phys. Chem., Neue Folge* **1982**, *133*, 93. (d) Kavarnos, G. J. *Top. Curr. Chem.* **1990**, *156*, 21.

(80) Marcus, R. A. *J. Chem. Phys.* **1956**, *24*, 966. Marcus, R. A. *Annu. Rev. Phys. Chem.* **1964**, *15*, 155. Marcus, R. A. *Rev. Mod. Phys.* **1993**, *65*, 599. Marcus, R. A. *Angew. Chem.* **1993**, *105*, 1161 (Nobel lecture).

(81) (a) Heitele, H. *Angew. Chem., Int. Ed. Engl.* **1993**, *32*, 359. (b) Gould, I. R.; Ege, D.; Moser, J. E.; Farid, S. *J. Am. Chem. Soc.* **1990**, *112*, 4290.

(82) (a) Closs, G. L.; Calcaterra, L. T.; Green, N. J.; Penfield, K. W.; Miller, J. R. *J. Phys. Chem.* **1986**, *90*, 3673. (b) Simmons, H. E.; Fukunaga, T. *J. Am. Chem. Soc.* **1967**, *89*, 5208.

(83) Note that redox potentials given in the literature often differ largely depending on the method employed (for differences in conversion constants, see e.g., Pavlishchuk, V. V.; Addison, A. W. *Inorg. Chim. Acta* **2000**, *298*, 97). Moreover, any simplifications made when employing the Weller equation have to be carefully considered.

(84) Note that these are the lifetimes of the complex(es) after 1 day of equilibration.

(85) Kollmannsberger, M.; Rurack, K.; Resch-Genger, U.; Daub, J. *J. Phys. Chem. A* **1998**, *102*, 10211.

(86) Kaden, T. A.; Kaderli, S.; Sager, W.; Siegfried-Hertli, L. C.; Zuberbühler, A. D. *Helv. Chim. Acta* **1986**, *69*, 1216.

(87) Similar proton-induced changes have been qualitatively reported by Buryakovskaya et al. for 3-quinolin-2-yl- and 3-pyrid-2-yl derivatives of **2b**.[50]

(88) Schugar, H. J. In *Copper Coordination Chemistry: Biochemical and Inorganic Perspectives*; Karlin, K. D., Zubieta, J., Eds.; Adenine: New York, 1983; p 43. Amundsen, A. R.; Whelan, J.; Bosnich, B. *J. Am. Chem. Soc.* **1977**, *99*, 6730.

(89) Elguero, J.; Jaquier, R. *Tetrahedron Lett.* **1965**, *17*, 1175.

(90)

$$f = \frac{mc_0^2 \ln 10}{\pi e^2 N_A n} \int_{\text{band}} \epsilon(\tilde{\nu})\, d\tilde{\nu} \qquad (17)$$

(ref 56). For a definition of parameters, see section 3.1.2.

(91) Notario, R.; Herreros, M.; Ballesteros, E.; Essefar, M.; Abboud, J.-L. M.; Sadekov, I. D.; Minkin, V. I.; Elguero, J. *J. Chem. Soc., Perkin Trans. 2* **1994**, 2341.

(92) Dewar, M. J. S.; Dougherty, R. C. *The PMO Theory of Organic Chemistry*; Plenum: New York, 1975; p 120.

(93) Kahmann, K.; Sigel, H.; Erlenmeyer, H. *Helv. Chim. Acta* **1965**, *48*, 295.

(94) log *K* values for M + L → ML. This is stressed by the log *K* values for Cu^{II} complexation with 2-thien-2-yl-pyridine (log $K = 0.2$. Sigel, H.; Wynberg, H.; van Bergen, T. J.; Kahmann, K. *Helv. Chim. Acta* **1972**, *55*, 610) and 4-pyrid-2-yl-imidazole (log $K = 8.76$. Eilbeck, W. J.; Holmes, F.; Phillips, G. C.; Underhill, A. E. *J. Chem. Soc. A* **1967**, 1161).

(95) Thompson, L. K.; Rendell, J. C. T.; Wellon, G. C. *Can. J. Chem.* **1982**, *60*, 514. Matthews, C. J.; Clegg, W.; Elsegood, M. R. J.; Leese, T. A.; Thorp, D.; Thornton, P.; Lockhart, J. C. *J. Chem. Soc., Dalton Trans.* **1996**, 1531.

(96) Pragst, F.; Siefke, B. *J. Prakt. Chem.* **1974**, *316*, 267.

(97) Knorr, L.; Laubmann, H. *Chem. Ber.* **1888**, *21*, 1205. Knorr's pyrazoline test is based on the reaction of 1,3,5-triphenyl-Δ^2-pyrazoline with Fe^{III} in acidic solution yielding an intense blue colour.

(98) The studies by Pragst et al. were carried out in acetonitrile as well. In the case of **2b** and Cu^{II}, a (weak) band at 22 400 cm^{-1} being characteristic for the intermediately formed radical cation[53] was also detected during our studies.

(99) Farha, F., Jr.; Iwamoto, R. T. *J. Electroanal. Chem.* **1964**, *8*, 55.

(100) Bourson, J.; Valeur, B. *J. Phys. Chem.* **1989**, *93*, 3871. Létard, J.-F.; Lapouyade, R.; Rettig, W. *Pure Appl. Chem.* **1993**, *65*, 1705. de Silva, A. P.; Sandanayake, K. R. A. S. *J. Chem. Soc., Chem. Commun.* **1989**, 1183.

(101) Concerning analytical applications, photooxidation of the 1,3,5-triaryl-Δ^2-pyrazolines has to be taken into account (Yamamoto, H.; Sano, Y.; Shirota, Y.; Seki, H.; Mikawa, H. *Bull. Chem. Soc. Jpn.* **1979**, *52*, 1533. Grimshaw, J.; de Silva, A. P. *J. Chem. Soc., Perkin Trans. 2* **1983**, 1679). Here, only for **1c** the occurrence of such a photoreaction could be verified when using comparatively high laser power (>9 kW pulse peak power) for excitation of a sample.

(102) de Silva, A. P.; Gunaratne, H. Q. N.; Kane, A. T. M.; Maguire, G. E. M. *Chem. Lett.* **1995**, 125. de Silva, A. P.; Gunaratne, H. Q. N.; Gunnlaugsson, T.; Nieuwenhuizen, M. *Chem. Commun. (Cambridge)* **1996**, 1967.

(103) Huston, M. E.; Haider, K. W.; Czarnik, A. W. *J. Am. Chem. Soc.* **1988**, *110*, 4460. de Silva, A. P.; Gunaratne, H. Q. N. *J. Chem. Soc., Chem. Commun.* **1990**, 186.

(104) Siebrand, W. *J. Chem. Phys.* **1967**, *46*, 440. Siebrand, W. *J. Chem. Phys.* **1967**, *47*, 2441.

(105) (a) Wagner, A.; Schellhammer, C. W.; Petersen, S. *Angew. Chem., Int. Ed. Engl.* **1966**, *5*, 699. (b) Kelly, G. P.; Leicester, P. A.; Wilkinson, F.; Worrall, D. R. *Spectrochim. Acta* **1990**, *46A*, 975. (c) Krasovitskii, B. M.; Bolotin, B. M. *Organic Luminescent Materials*; VCH: Weinheim, Germany, 1988; p 197. (d) Krasovitskii, B. M.; Bolotin, B. M. *Organic Luminescent Materials*; VCH: Weinheim, Germany, 1988; p 200. (e) Wiley, R. H.; Jarboe, C. H.; Hayes, F. N.; Hansbury, E.; Nielsen, J. T.; Callahan, P. X.; Sellars, M. C. *J. Org. Chem.* **1958**, *23*, 732. (f) Sandler, S. R.; Loshaek, S.; Broderick, E.; Tsou, K. C. *J. Phys. Chem.* **1962**, *66*, 404.

(106) Edward, J. T. *Chem. Ind. (London)* **1956**, 774.

(107) Herbich, J.; Kapturkiewicz, A. *J. Am. Chem. Soc.* **1998**, *120*, 1014.

(108) McRae, E. G. *J. Phys. Chem.* **1957**, *61*, 562.

(109) The corresponding values obtained for **1c** by global analysis of 8 decays are 0.03 ns ($\langle a_{rel} \rangle = 0.82$) and 0.34 ns.

(110) Atomic deviations from the planes (Å). **1b**: plane 1 = 0.043 N(1), −0.003 N(2), −0.037 C(3), 0.055 C(4), −0.057 C(5); plane 2 = 0.002 C(6), −0.003 C(7), 0.002 C(8), 0.002 C(9), −0.003 C(10), 0.001 C(11); plane 3 = −0.002 C(12), −0.011 N(13), 0.018 S(14), −0.005 C(15), −0.003 C(16), 0.008 C(26), 0.012 C(27), −0.005 C(28), −0.012 C(29); plane 4 = 0.001 C(18), −0.001 C(19), 0.000 C(20), 0.001 C(21), −0.001 C(22), 0.000 C(23). **2a**: plane 1 = 0.063 N(1), −0.024 N(2), −0.026 C(3), 0.057 C(4), −0.070 C(5); plane 2 = 0.012 C(6), −0.012 C(7), −0.002 C(8), 0.015 C(9), −0.014 C(10), 0.001 C(11); plane 3 = −0.001 C(12), 0.003 C(13), −0.002 C(14), 0.000 C(15), 0.002 C(16), −0.002 C(17); plane 4 = −0.017 C(18), 0.013 C(19), 0.002 C(20), −0.013 C(21), 0.009 C(22), 0.006 C(23). **3**: plane 1 = 0.057 N(1), −0.011 N(2), −0.041 C(3), 0.066 C(4), −0.072 C(5); plane 2 = −0.009 C(6), 0.003 C(7), 0.003 C(8), −0.002 C(9), −0.003 C(10), 0.009 C(11); plane 3 = 0.015 C(12), −0.009 N(13), 0.011 S(14), −0.014 C(15), −0.006 C(16), −0.007 C(26), 0.017 C(27), 0.017 C(28), −0.025 C(29); plane 4 = 0.003 C(18), −0.001 C(19), 0.004 C(20), −0.009 C(21), 0.010 C(22), −0.007 C(23).

(111) $\langle \tau_f \rangle = \sum_i a_i \tau_i / \sum_i a_i$

(112) Zweig, A.; Hodgson, W. G.; Jura, W. H. *J. Am. Chem. Soc.* **1964**, *86*, 4124. Their published value of −1.76 V vs SCE was adjusted using a conversion constant of $Fc/Fc^+ + 0.31$ V = SCE.[83]

(113) Due to the heterocyclic donor atoms being present in the chromophore (and in form of the nitrogen atom in the receptor), at higher concentrations, i.e., at $x_{M/L} > 100$, slight spectroscopic changes are observable for other heavy and transition metal ions such as, e.g., Ni^{II} as well. However, the occurrence of these trace metal ions at such concentrations is barely found in matrices where fluorescence sensing is commonly employed.

(114) (a) Shannon, R. D. *Acta Crystallogr.* **1976**, *32A*, 751. (b) Frensdorff, H. K. *J. Am. Chem. Soc.* **1971**, *93*, 600. (c) Dalley, N. K. In *Synthetic Multidentate Macrocyclic Compounds*; Izatt, R. M., Christensen, J. J., Eds.; Academic: New York, 1978; p 207.

(115) (a) Jonker, S. A.; Verhoeven, J. W.; Reiss, C. A.; Goubitz, K.; Heijdenrijk, D. *Recl. Trav. Chim. Pays-Bas* **1990**, *109*, 154. (b) Pauling, L. *J. Am. Chem. Soc.* **1927**, *49*, 765. (c) Jonker, S. A. Ph.D. Thesis, University of Amsterdam, Amsterdam, 1989.

(116) Rorabacher, D. B.; Martin, M. J.; Koenigbauer, M. J.; Malik, M.; Schroeder, R. R.; Endicott, J. F.; Ochrymowycz, L. A. In *Copper Coordination Chemistry: Biochemical and Inorganic Perspectives*; Karlin, K. D., Zubieta, J., Eds.; Adenine: New York, 1983; p 167.

(117) (a) Hinze, J. *Fortschr. Chem. Forsch.* **1968**, *9*, 448. (b) Allred, A. L. *J. Inorg. Nucl. Chem.* **1961**, *17*, 215. (c) Allred, A. L.; Rochow, E. G. *J. Inorg. Nucl. Chem.* **1958**, *5*, 264.

(118) Nieboer, E.; Richardson, D. H. S. *Environ. Pollut. Ser. B* **1980**, *1*, 3.